Modelling and Optimization of a Pilot-Scale Entrained Flow gasifier using Artificial Neural Networks

by

Han Wang

A thesis
presented to the University of Waterloo
in fulfillment of the
thesis requirement for the degree of
Master of Applied Science
in
Chemical Engineering

Waterloo, Ontario, Canada, 2020

AUTHOR'S DECLARATION

I hereby declare that I am the sole author of this thesis. This is a true copy of the thesis, including any required final revisions, as accepted by my examiners.

I understand that my thesis may be made electronically available to the public.

Abstract

Recently, integrated gasification combined cycle power generation system (IGCC) has been considered as an attractive technology which is capable of curbing CO_2 emissions and reducing impact on environment due to the increasing global carbon dioxide emissions from combustion of fossil fuels in these decades. IGCC is an advanced power system consisting of two main sections, namely the gasification and purification part and the gas-steam combined cycle power generation part. There has been substantial interest in studying the modeling and optimization of the gasifier performance in IGCC to improve the efficiency of fuel and power generation, versatility, reliability and economics in IGCC systems. Previous studies on modelling for gasification such as computational fluid dynamic (CFD) models and reduced order models (ROM) have been presented; however, these modelling approaches are not suitable for conducting optimization since they are too complex and computationally intensive. Recently, there have been an increasing number of studies where artificial neural networks (ANN) and recurrent neural networks (RNNs) have been used to model different applications in chemical engineering. This is mostly because neural networks are suitable for describing the complex nonlinear multifactorial systems at low computational costs.

The aim of this study is to present the construction and validation of both ANN and RNN models to accurately and efficiently predict both steady state and dynamic performance of a pilot-scale gasifier unit. The corresponding ANN and RNN models' performance were validated using data generated from a gasifier's ROM. After validation of ANN and RNN models, optimization studies on the steady state and transient performance of the gasifier were performed under different scenarios, e.g. co-firing and load-following. In the optimization studies at steady state, results show that increasing the peak temperature limitation of the gasifier can promote a high maximum carbon conversion, and it seems unlikely to improve H_2 production significantly without reducing the carbon conversion within the gasifier. In the dynamic optimization studies, the results from

load-following scenario show that increasing the peak temperature limitation of the gasifier can lead to higher CO compositions at the outlet of the gasifier. For the co-firing scenario, the results show that an increase on the coal to pet-coke ratio can promote a higher carbon conversion in the gasifier. These optimization studies further showcase the benefit of the ANN and RNN models, which were able to obtain relatively accurate predictions for the gasifier similar to the results generated by ROM at a much lower computational cost.

Acknowledgements

I would like to thank Professor Luis Ricardez-Sandoval, for giving me with the chance to pursue a MASc degree at the University of Waterloo and also for all the support, guidance and advice throughout this work.

I would like to extend my appreciation to the readers of my thesis.

And I also make an acknowledgement to my parents and my grandparents who always support me, love me and encourage me to pursue for a graduate degree. I would like to thank auntie Shuang Ma and her families, for helping me feel loved and welcome in Canada. And last but not least, to my group members for helping me feel warm and happy.

Dedicated to my family

Table of Contents

List of Figures

List of Tables

Nomenclature

English symbols

ANN	Artificial neural network
A	Area (m^2)
$\mathbf{b}$	Vector of biases
b_i	Bias applied to ith neuron
CCS	Carbon capture and storage technology
CFD	Computational fluid dynamic
CPU	Central processing unit
CO_2	Carbon dioxide
CO	Carbon monoxide
COS	Carbonyl sulfide
CSTR	Continuous stirred tank reactor
C	Concentration ($mole/m^3$)
C_P	Heat capacity (J/kg/K)
D	Diffusivity (m^2/s)
DSZ	Down-stream zone
ERZ	External recirculation zone
F'	Volumetric force (N/ m^3)
f	Transfer function
f_1	Nonlinear activation sigmoid function
f_2	Linear function
g	Gravitational acceleration (m/s^2)
g	Predictor function
H_2	Hydrogen
H_2O	Water
H_2S	Hydrogen sulfide
H	Enthalpy (J/kg)
HS	Heat source
h	Convection coefficient ($W/m^2/K$)
$h_{w,b}$	Hypothesis nonlinear function
IGCC	Integrated gasification combined cycle

JEZ	Jet expansion zone
J	Objective function of the training process
k	Thermal conductivity (W/m/K)
MSE	Mean squared error
M	Mass flow (kg/s)
m	Mass (kg)
m′	Mass flux (kg/m^2/s)
NARX	Autoregressive network with exogenous inputs model
N	Density of particle (1/m^{-3})
N_2	Nitrogen
n	Number of data pairs
n_u	Discrete time index of time delay of input signal
n_y	Discrete time index of time delay of output signal
O_2	Oxygen
OF_j	Objective functions
OF_1	First objective function for the load-following optimization
OF_2	Second objective function for the load-following optimization
PFR	Plug flow reactor
$\mathbf{P}$	Vector of key input parameters for ANN model
$\mathbf{P}'$	Vector of key input parameters for RNN model
$\mathbf{P}_{nom}$	Gasifier nominal operating conditions
$\mathbf{P}_{max}$	Upper bounds on key input parameters
$\mathbf{P}_{min}$	Lower bounds on key input parameters
$\mathbf{P}^{t0}$	Initial conditions
P_1	Injected fuel flowrate (kg/h) for ANN model
P_2	Oxygen flowrate (kg/h) for ANN model
P_3	Nitrogen flowrate (kg/h) for ANN model
P_4	Steam flowrate (kg/h) for ANN model
P_5	Initial fuel temperature (K) for ANN model
P_6	Mass fraction of ash for ANN model
P_7	Mass fraction of volatiles for ANN model
P_8	Mass fraction of moisture for ANN model
P'_1	Injected fuel flowrate (kg/h) for RNN model

P_1^{t0}	Initial operating condition of the fuel flowrate
P'_2	Oxygen flowrate (kg/h) for RNN model
P'_3	Nitrogen flowrate (kg/h) for RNN model
P'_4	Steam flowrate (kg/h) for RNN model
P'_5	Limestone (CaO) flowrate (kg/h) for RNN model
P'_6	Mass fraction of ash for RNN model
P'_7	Mass fraction of volatiles for RNN model
P'_8	Mass fraction of moisture for RNN model
Q'	Heat flux (W/m^2)
RNN	Recurrent neural network
ROM	Reduced order model
$\mathbf{R}$	Dimensions of the inputs
r	Radius (m)
$\mathbf{S^1}$	Dimensions of the weights
$\mathbf{S^2}$	Dimensions of the bias
TPD	Tonne per day
T	Temperature (K)
$\mathbf{T}$	Vector of key output parameters
T_1	Carbon conversion
$T_{1,max}$	Maximum gasifier carbon conversion
$T_{1,min}$	Minimum gasifier carbon conversion
T_2	Molar composition of CO in the syngas
T_2^*	Pre-specified target set-up point for CO
T_3	Molar composition of H_2 in the syngas
$T_{3,max}$	Maximum gasifier H_2 molar fraction
$T_{3,min}$	Minimum gasifier H_2 molar fraction
T_4	Peak temperature in gasifier (K)
$T_{4,max}$	Maximum allowable peak gasifier temperature (K)
T_5	Temperature at thermocouple 1 (K)
T_6	Temperature at thermocouple 2 (K)
T_7	Temperature at thermocouple 3 (K)
T_8	Temperature at thermocouple 4 (K)

T_9	Maximum refractory temperature (K)
T_{10}	Refractory temperature at outlet (K)
T_{11}	Slag viscosity (Pa s)
T_{12}	Slag thickness (mm)
$T_{12,max}$	Maximum allowable slag thickness (mm)
$\boldsymbol{t}$	Discrete time step
t_i	Discrete time points in optimization
u	Velocity (m/s)
u	Input signals
w	Multi-objective significance weight
$\mathbf{w}$	Vector of weights
$\boldsymbol{W_1}$	Matrices of network weights from the input layer to the hidden layer
$\boldsymbol{W_2}$	Matrices of network weights from the hidden layer to the output layer
$w_{i,j}$	Weight connected jth input parameter and ith neuron in hidden layer
x_j	Input value of the jth input parameter
$x^{(i)}$	ith input
$y^{(i)}$	ith target output
y	Actual output of RNN model
$\hat{\boldsymbol{y}}$	Target output of RNN model
z	Axial domain (m)

Greek symbols

α	Learning rate
ε	Volume fraction
δ	Slag thickness (m)
Δt	Length of the sampling interval
ξ_i	Linear weights function for the ith neuron
ρ	Density (kg/m^3)
$\emptyset$	Function of current and delayed inputs
θ	Ratio of coal to pet-coke
θ_{max}	Maximum of ratio of coal to pet-coke
θ_{min}	Minimum of ratio of coal to pet-coke

Subscripts

conv	Convection
cs	Cross section
eff	Effective
g	Gas
het	Heterogeneous reaction
hom	Homogeneous reaction
p	Particle

Chapter 1
Introduction

Nowadays, there is a global interest to reduce CO_2 emissions and other heat-trapping gases to the atmosphere to curb global warming. Global CO_2 emissions from the combustion of fossil fuels are anticipated to exceed 6 billion tonnes by 2035[1]. At present, approximately one third of total CO_2 emissions are produced from coal-fired power generation plants, making it the second largest production source of greenhouse gases. It is expected that coal will persist as the main fuel for power generation in 2035, and that coal proportion of the total distribution to CO_2 emissions will remain relatively unchanged between now and then[2]. This situation is expected to cause the worldwide capacity of coal-fired power plants to increase by approximately 40%. Hence, the demand for coal-based power plants is anticipated to increase CO_2 emissions and thus causing a negative impact on global warming. Sustainable coal-fired power plants that can operate under near-zero emissions are thus needed to fight against climate change and global warming. As a result, there is currently an urgent need to develop and implement efficient carbon capture and storage (CCS) technologies[3]. However, a recent report from the World's first commercial-scale CO_2 capture facility in SaskPower's Boundary Dam power plant, Canada, showed that a 20% reduction in power generation was required to operate the CO_2 capture plant[2]. Therefore, more efficient power production technologies need to be developed to compensate for the expenses associated with CO_2 capture systems.[4]

Integrated gasification combined cycle (IGCC) plants are advanced power systems consisting of a gasification and a quench unit, a water-gas shift reactor, a purification unit, a gas turbine, a heat recovery steam generator, a steam turbine and an air separation unit. IGCC plants has been considered as one of the most efficient power plants since they can reduce the production of solid wastes and lower sulfide and nitride emissions; also they require less expensive gas-cleaning equipment and they possess high fuel flexibility.[5] Recently, more attention has been placed on

the development of efficient gasification units that can handle different amounts of loading and feedstock types. It has been widely recognized that fuel flexibility allows power plants to adapt to changes in fuel and retain an effective cost energy production scheme.

The gasification unit is perhaps the most important process in an IGCC plant. Fuel, oxygen and steam are fed into the gasifier to produce raw syngas, which mainly consist of CO, H_2, and CO_2. The mixture of raw syngas is promptly cooled in quench vessels; subsequently, most of the H_2S and COS impurities are removed via a gas cleanup unit and then solidified for transportation. After impurity removal, clean syngas is sent to the gas turbine and then to a heat recovery steam generator.[6] Therefore, there has been crucial interest in studying the performance of IGCC gasification unit in order to improve the versatility of fuel and the operability, controllability and efficiency of IGCC power generation systems.[7]

Computational fluid dynamic (CFD) models are commonly used to simulate the performance of the gasifiers because of their ability to explicitly describe mixing flows in this system and therefore provide sufficiently accurate predictions.[8,9,10] These models can provide meaningful and comprehensive insights about the overall design and performance of the gasifier; however, although CFD models are accurate and provide a relatively detailed outlook compared to other gasification simulation models, they are often found to be computational intensive, which can significantly limit their implementation for process optimization, online monitoring, and process control applications.[11] This has motivated the development of alternative, computationally efficient modelling techniques. Reduced order models (ROMs) are an alternative approach that can capture the essential features of multi-phase flow structure inside the gasifier at reduced computational costs.[12,13] However, although ROMs require substantially lower computational costs compared to CFD models, they are still computationally expensive and may not be applied for process optimization, monitoring and on-line control purposes.

Artificial neural network (ANN) is another effective modelling approach that can be implemented to predict the performance of gasification unit in IGCCs at reduced computational costs. ANN are inspired by the biological neural networks in human brain which consist of robust mathematical model to produce relational patterns between input and output parameters for nonlinear multifactorial systems.[14] In addition, recurrent neural network (RNN) is a class of ANN that are especially suitable for simulating time series systems such as the dynamic operation of a gasifier. After the training process, both ANN and RNN model can perform prediction and generalization with sufficient accuracy at low computational costs. Recently, there has been an increasing number of studies where artificial neural network has been used to predict the performance of multiple applications in chemical engineering, e.g., transport of the precursor gas phase of a thin film surface, simulation of a thin film formation by chemical vapour deposition, synthesis, design, control, scheduling and optimization of process control engineering.[15,16,17] However, to the authors' knowledge, both ANN and RNN have not been previously used for modelling and optimization of entrained flow gasifiers in IGCC system. As a result, ANN and RNN model are required to overcome the limitations imposed by computationally intensive CFD model and ROM in optimization problems involving the gasification unit in IGCC plants.

1.1 Research objectives

The aim of this study is to develop ANN and RNN models to describe and predict the behavior between the main features of IGCC gasification units in both the stationary and transient domains. The proposed models were trained and validated using sets of input and output data generated from a ROM model previously developed within our research group.[12] Subsequently, the fully-developed nonlinear ANN and RNN models are used to perform optimization on the stationary and transient operating conditions of a gasifier with the aim to gain a deeper understanding on

the optimal operation of these units under common scenarios. The specific objectives of the current study are as follows:

- Develop an ANN model to describe the steady state performance of a pilot-scale entrained flow gasifier. The validated ANN model would be subsequently embedded within optimization formulations to determine the operating conditions that would maximize the efficiency of this unit under different operational scenarios.
- Develop a recurrent neural network (RNN) to accurately and efficiently predict the dynamic performance of the pilot-scale gasifier. The performance of the RNN will be compared to a ROM model, which has been previously validated using experimental data and data obtained from CFD simulations. The RNN model will be embedded within an optimization formulation to investigate the optimal operation of a gasifier under the most common dynamic operating scenarios encountered in gasification such as load-following and co-firing.

The contribution of this work is to illustrate the performance of the gasification unit using artificial neural networks and showcase their benefits in terms of accuracy in the predictions and computational efficiency.

1.2 Outline of this study

This thesis is organized as follows:

Chapter 2 presents a literature review on the most common modelling methods to describe the performance of gasification systems, including CFD, ROM and ANN models. The goal of this review is to provide insight into the current models and identify the advantages and benefits of ANN modelling in the literature on the steady-state and dynamic simulation of gasification units.

Chapter 3 presents the development and validation of an ANN model that can predict the performance of a pilot-scale gasification unit at steady state. During the ANN training process, eight backpropagation methods have been compared to select the most suitable training algorithm for the ANN model. Subsequently, the ANN model was considered for the optimization of the gasification unit, i.e., maximization of the carbon conversion and maximization of both carbon conversion and hydrogen gas.

Chapter 4, a recurrent neural network (RNN) model was developed to capture the transient operation of the pilot-scale gasifier. The resulting RNN was validated using the data generated by dynamic ROM, which was validated using CFD simulations and experimental data taken from an actual pilot-scale gasification unit. The recurrent neural network model was identified using a new method of generating data, which is a combination of two common operating scenarios in gasification (i.e., load-following and co-firing). In addition, dynamic optimization studies on the performance of the gasifier were conducted under load-following and co-firing.

Chapter 5 presents the conclusions drawn from this study and a brief overview of potential areas of future research.

Chapter 2
Literature Review

This chapter presents the relevant literature on the different modeling methods and optimization approaches considered for gasification units. The scope of this review will include a general overview of IGCC power plant, the role of gasification process in IGCC and a brief description on the gasification unit. Additionally, this chapter will review the status of modelling and optimization on gasifiers and introduce artificial neural network methods including construction, algorithms and applications on energy systems in the chemical engineering field. This review aims to highlight the need for research in modelling and optimization of steady state and dynamic performance of gasification unit using ANN; in particular, the features of implementing dynamic optimization to identify optimal operating conditions for this gasification process.

2.1 Gasification unit in IGCC plant

2.1.1 Overview of IGCC power plant

Integrated gasification combined cycle (IGCC) power plants are recognized as one of the most attractive methods of coal-based power production with considerably low CO_2 emissions.[18] In IGCC systems, the impurity removal process is included, in which most of H_2S and COS are removed. Comparing to other power generation plants, the main benefits of IGCC are lower solid wastes production, higher fuel flexibility, higher efficiency, low pollution gas emissions.[19]

A brief description of the process of a typical IGCC plant with CO_2 capture is shown in Figure 1. In IGCC plants, fuel, oxygen, and steam are fed to the gasification unit to produce raw syngas mainly consisting of CO, H_2, and CO_2. This mixture is promptly cooled in quench vessels and is sent to a water-gas shift reactor before the gas cleaning unit removes the carbon in the form of

CO_2. Subsequently, particulates and sulfur impurities are removed via a gas cleanup unit. After impurity removal, the clean syngas is fed to the gas turbine and then sent to a heat recovery steam generator coupled with a steam turbine.

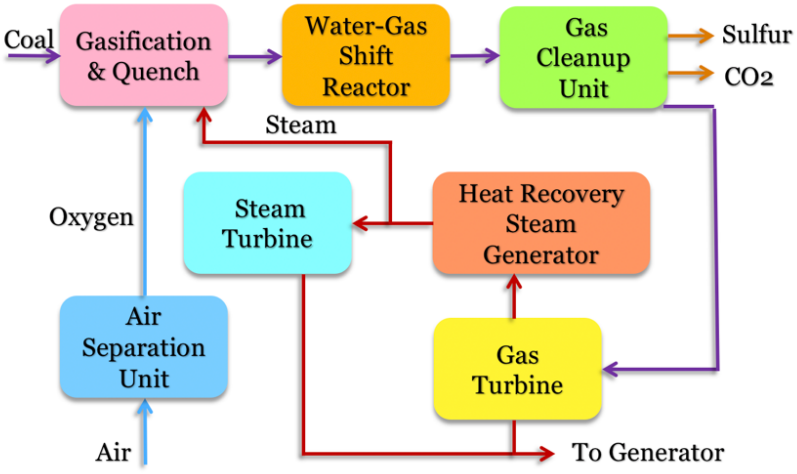

Figure 1. Brief process flowsheet of IGCC power plant

Multiple studies have been conducted to improve the efficiency, availability and economics of power generation of IGCC system.[20,21,22,23] The current emphasis is placed on the entrained-flow gasifier's operation for improvement and development of IGCC power plant. The gasification unit in IGCC plant is required to have high flexibility to change flowrate and type of feed, since the development and commercialization of IGCC power plants are required to be improved in terms of technology and equipment selection for different feedstocks.[24] In addition, the efficiency of the gasification unit also affects the operation of the rest of the IGCC plant. Therefore, as gasification is the key process of IGCC plant, the focus of this research is on the modelling and optimization of the operating conditions for both the steady state and dynamic performance of entrained-flow gasifiers in IGCC plants.

2.1.2 Gasification technologies

Gasification is a process in which a fossil fuel-based carbonaceous feed is transformed into gaseous products such as, carbon monoxide (CO), hydrogen (H_2), and carbon dioxide (CO_2), commonly referred to as raw syngas. The most important reactions taking place in this process involve coal pyrolysis reaction, char and volatile combustion and sulfur reaction. During gasification, the fuel is blended with steam and oxygen and fed into the gasifier where fuel is dried and decomposed to volatiles, char and ash; the later process is referred to as coal pyrolysis. After this process, the main volatile products, combustible gases such as hydrogen, carbon monoxide, methane and ethane are produced. All these combustible gases react with oxygen to produce heat and provide the energy required by the heterogeneous char gasification reactions to produce hydrogen, carbon monoxide and methane. Due to the reactions taking place in the unit, the sulfur content in the fuel is transformed into $H_2S_{(g)}$.[6,20]

In the industry, there are mainly four types of gasification units that can be found, i.e., fixed-bed, fluidized-bed, entrained-flow and molten-bath gasifiers. Each type of gasification system presents some advantages and disadvantages on the performance, operating conditions and feed availability as illustrated in Table 1. In terms of fixed-bed gasifiers, it has benefits of consuming less oxygen (O_2), simple construction, low pressure dropping and high carbon conversion; however, this type of gasifier has higher methane content in the outlet and it is hard to control the temperature distribution along the length of the gasifier.[3] In fluidized-bed gasifiers, the reaction rate is moderate due to good mixing of reactants and the temperature distribution along the gasifier is easier to control; however, these systems present high erosion rate of the bed material surfaces inside the gasifier, higher dust load due to the entrainment of particles and agglomeration for certain type of fuels.[3] Molten-bath gasifier is capable of both caking and non-caking coke; however, their disadvantages are high oxidation rate and complicated regeneration system.[20] Regarding entrained-flow gasifiers, they have high throughput and efficiency with very short

residence time (i.e., in the order of seconds or less) and are suitable for all coal types; however, they require a large amount of oxidant; also, the combustion temperature is high inside these gasifiers, which has the potential to damage the refractory material of this equipment.[8]

Table 1. Advantages and disadvantages of different types of gasifiers[25]

Gasifier types	Advantages	Disadvantages
Fixed-bed gasifier	Consume less oxygen (O_2) Simple construction Low pressure dropping High carbon conversion	Higher methane content in outlet Hard temperature distribution control
Fluidized-bed gasifier	Moderate reaction rate Good mixing of reactants Easy temperature distribution control	High erosion rate of surfaces High dust load
Entrained-flow gasifier	High throughput and efficiency Short residence time High flexibility of fuel types	Large amount of oxidant High combustion temperature
Molten-bath gasifier	Capable of both caking and non-caking coke	High oxidation rate Complicated regeneration system

Among the different types of gasifiers, entrained-flow gasifiers are the most common commercial gasifiers currently in the market since it has higher throughputs compared to other gasification equipment. Hence, the present research focused on this type of gasifiers. In particular, this study focused on a pilot-scale entrained flow gasifier owned by CanmetENERGY (Natural Resources Canada). As illustrated in Figure 2, this pilot-scale gasifier's diameter and length are 0.21 m and 2.2 m, respectively. Fuel, steam (H_2O), oxygen (O_2) and nitrogen (N_2) are fed into the gasifier to

produce raw syngas. At the gasifier inlet, oxygen is injected through the burner by eight jets and mixed with the fuel stream at a high velocity. Steam preheated to 500 K is passed through the outer burner annulus at a low velocity, and the fuel is carried through the reactor inlet by a stream of nitrogen carrier gas. The gasifier is lined with refractory and insulation materials in order to reduce its heat loss, as it has a large surface area to volume ratio. There are more details about this gasification unit which can be found elsewhere.[26]

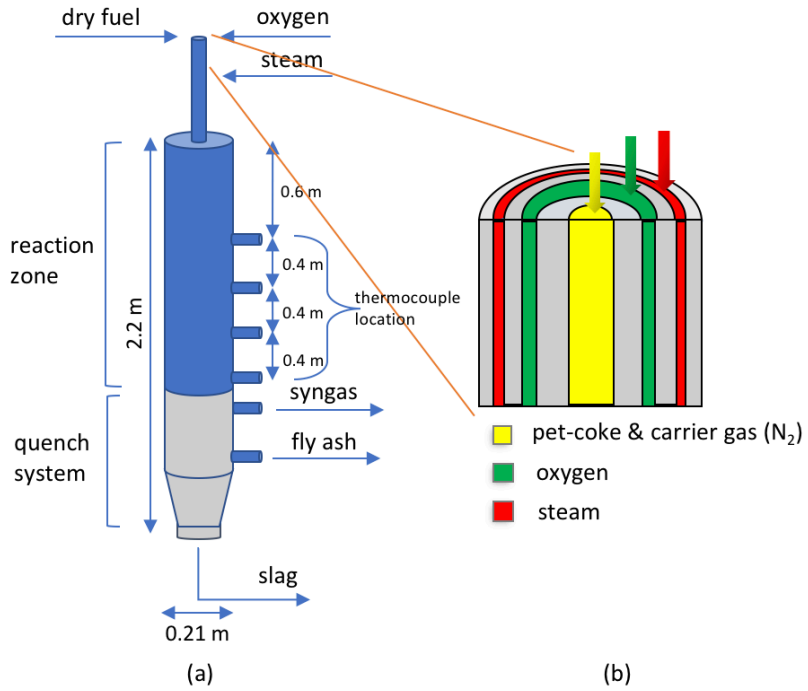

Figure 2. (a) Configuration of the pilot-scale gasifier; (b) Inflow structure of the gasifier and its feeds

To advance the technological development of gasification units, a deeper understanding of gasifier's feed flowrates and the coal feed types on the operability of this unit are needed to obtain an optimal and more efficient performance of the gasifier under different conditions, e.g., load following and co-firing. Since it is costly to conduct experimental tests on the entrained flow gasifier, computational models are required to assess the performance and economics of the

gasification units at different operating conditions. Therefore, a review of the modeling approaches used to simulate entrained flow gasifiers is presented next.

2.2 Modeling of gasification process

In an IGCC power plant, the complex integration of the different units is reflected in the responses of a unit to external and internal disturbances and the interaction between each of the units thus affecting the operability, controllability and efficiency of the IGCC. Since an IGCC power plant is one of those technologies that has the potential to balance the power distribution networks and compensate for variable electricity supply, the responses of the gasifier and other equipment can lead to undesired operational fluctuations to different load demands.[27,28,29] Therefore, IGCC plants need to have high flexibility to change the feed flowrate when combined with alternative energy sources and being able to maintain continuous operation with different solid fuels to meet the targets of compensating for variable electricity supply.[13] However, it is relatively challenging to achieve flexibility and incorporate variability for an IGCC plant due to the high complexity and interconnectivity of the different units involved in this process. As a result, there is a need to study the transient behaviour of each component of the IGCC in order to gain insight into the dynamic response of the units under different disturbances, such as changes to the fuel load and variability in feed composition. Previous studies have evaluated and analysed the dynamic performance of key IGCC power plant units such as the air separation and CO_2 capture units;[7,30] however, studies focused on the dynamic behaviour of other critical IGCC components such as the gasification unit are limited. There are three common approaches that can be employed to simulate the behaviour of the gasification process, i.e., computational fluid dynamics (CFD), reduced order model (ROM) and more recently artificial neural network (ANN) models. Each of these modelling approaches is discussed next.

2.2.1 Computational fluid dynamics (CFD)

Computational fluid dynamics (CFD) models are often used to simulate gasifiers because of their ability to explicitly handle gasification flows and mixing and therefore provide sufficiently accurate predictions. In a CFD model, detailed multi-phase sub-models are often implemented to simulate the flow patterns and complex processes; hence, they have been widely used to investigate different types of gasification unit's performance, including fluidized-bed gasifiers, entrained flow gasifiers, slagging gasifiers. Xue and Fox presented a computational fluid dynamics model for biomass gasification process taking place in fluidized-bed gasifier simulations. The physical and chemical processes of multi-phase gasification and interaction of different phases are modeled within a multi-fluid framework derived from kinetic theory of granular flows.[31] Slezak et al. presented a CFD simulation of a commercial-scale entrained-flow gasifier to study the effects of simulating both the coal particle density and size variations.[32] Sze Zheng Yong and Ahmed Ghoniem developed a steady state model based on CFD to describe the flow and heat transfer characteristics of slagging gasification unit.[33] Most notably, Fletcher et al. developed a CFD model to simulate the flow and reaction in an entrained flow gasifier that they built based on the CFX package, which is a useful tool for gasifier design and analysis.[9] E. H. Chui et al. described the development of a CFD-based simulation for commercial coal gasification technology and its implementation; those authors used that model to capture physical phenomena and supplement the experimental program for better understanding of the coal gasification processes.[8] Fernando et al. developed a two dimensional CFD model to simulate the dynamic performance of a moving bed updraft biomass gasifier.[34] Murgia et al. developed a comprehensive CFD model to simulate the fixed bed gasification process within an air-blown updraft coal gasifier, which characterize the complex behaviour of time-dependent sub-process where coal drying, de-volatilization and char reactions take place.[35] Although CFD models are accurate and provide a more detailed outlook compared to other gasification simulation models, they are often found to be computationally

intensive, which can significantly limit their implementation for the dynamic optimization of this unit.

2.2.2 Reduced order model (ROM)

To reduce the computational costs associated with the modelling of gasification units, recent studies have shown that the development of one-dimensional ROMs describing the important features of gasification unit is a computationally attractive approach to study the steady state and transient behaviour of nonlinear energy systems. ROMs require much lower computational effort compared to CFD models, accounting for the most important features of gasification process. These ROMs can be used to provide detailed information about the multi-phase flow structure of a gasification unit such as its solid particle concentration, composition, and temperature distribution along the length of the gasifier by developing a reactor network based on the mixing or laminar flow characteristics. Inside each reaction zone, the one-dimensional governing equations of gas and solid phases for mass, energy, and momentum are solved for each zone to provide a distribution of different properties. Gazzani et al. described the development of a reduced order model for the Shell-Prenflo gasifier in IGCC, which is used for chemicals and power production due to its high efficiency and compatibility with a wide range of coal quality.[38] Yang et al. developed a detailed model using ROM for a slurry-feed membrane wall entrained flow gasifier with two-stage oxygen supply in order to obtain an in-depth understanding of the gasifier and achieve optimal design and operation.[39] The same authors established a dynamic ROM gasifier model including slag flow behaviour simulation using a network of reactors, in which the reactor is divided into several zones based on the flow characteristics in the gasifier.[40] In Li et al. study, a reduced order model (ROM) of a commercial-scale opposed multi-burner gasifier is presented based on a network of reactors. In that study, the effects of particle size on the temperature and carbon conversion were discussed.[41] Monaghan and Ghoniem developed a comprehensive

dynamic ROM using a network of ideal chemical reactors in series to approximate the fluid mixing and recirculation inside entrained flow gasifiers and study its transient response under dynamic operation.[6] Sahraei et al. proposed a reactor network ROM which utilizes plug flow reactor (PFR) and continuous stirred tank reactor (CSTR) models to simulate the different zones inside an entrained-flow gasifier. This ROM model is built up to represent CanmetENERGY's pilot-scale entrained-flow gasifier described in the previous section and that will be used in this research. That model was developed based on the streamlines of multi-phase flow via conservation equations describing the momentum, heat and mass transfer inside the gasifier.[13] With regards to the computational cost, the ROM model required on average about 257 s of CPU time per simulation (Intel® Core™ i7-4770 CPU @ 3.40Hz, 3392 Mhz, 4 Core(s), 8 Logical Processor(s)).[42] However, even though the ROMs require substantially lower computational costs compared to CFD models, they still require considerable numerical analysis and thus they are still computationally expensive for optimization, online monitoring and control purposes.

2.2.3 Artificial neural network models

Artificial neural networks (ANN) are another modelling method that can be used to predict the performance of the gasification unit in IGCCs at reduced computational costs. ANN are inspired by the biological neural networks in a human brain, and they utilize robust mathematical models to produce cause-effect relational patterns between complex data systems such as nonlinear multifactorial systems.[43]

ANN have been used to model numerous applications in Chemical Engineering;[16,15] in particular, there have been a handful of works that have applied ANN to gasification systems. Ongen et al. proposed an ANN model to observe variations in the syngas related to operational conditions in a tannery industry wastewater treatment sludge gasification system.[46] Mikulandric et al. analyzed the possibilities of neural networks to predict process parameters of a fixed bed gasifier in a

biomass gasification process with high speed and accuracy.[47] Puig-Arnavat presented an ANN model for biomass gasification in fluidized bed reactors.[48] In a study reported by Guo B et al., an artificial neural network model has been developed to simulate this biomass gasification processes in fluidized bed gasifier under high pressure in order to obtain a comprehensive gasification profile.[49] George Joel et al. developed an ANN model for a gasification process which generate energy from renewable and carbon-neural biomass based on extensive data obtained from experimental investigations.[50]

The studies mentioned above are related to modelling the steady state performance of a gasifier. Recurrent neural network (RNN) is a class of ANN that are especially suitable for simulating time series dynamic systems. Traditional artificial neural networks (i.e., the feedforward neural network) are static approximators and consequently have difficulties to describe the transient operation of highly complex chemical systems.[51,52] Thus, in order to design discrete-time neural networks for transient systems, it is required to implement a neural network architecture that can learn from the current state of the system when predicting future states. The architecture of an RNN contains cyclic connections between specific nodes that allows the network to remember and learn from its own predictions, which is well-suited to model temporal data such that those that emerges in dynamic process systems. After sufficient training, the RNN can perform prediction and generalization with sufficient accuracy at high speed and can achieve greater accuracy at lower training costs compared to feed-forward neural networks.[53] Nowadays, there have only been minimal studies associated with the application of RNN to describe the dynamic operation of energy production systems, and even fewer studies have developed RNN for gasification systems. Chin-Hsing Cheng and Jian-Xun Ye discussed an energy recovery system of the electric motorcycle using artificial neural network to improve the dynamic performance and life cycle of batteries.[54] Velappagari Sekhar proposed an RNN-based controller to improve the low-voltage ride-through ability of the grid-connected wind energy conversion system.[55] Souza et

al. modelled a biomass gasification process in a fluidized bed gasifier based on the concepts of ANN to correlate between the composition of the produced gas and the characteristics of different biomasses for several operating conditions.[56] Pandey et al. developed an ANN-based modelling approach to estimate the low heating value of the gasification products.[57] In a study performed by Kallol Roy et. al., a model based on RNN was presented to determine the scheduling of a micro grid system and analyzed the technical and economic time-dependent constraints.[58] Mikulandric et. al presented a dynamic neural network-based model for a biomass gasification process and compared its performance against experimental data.[59]

Moreover, only very few studies in the energy sector have shown that the models based on ANN can be embedded within optimization formulations to improve the efficiency of energy systems. Wang Jianlong and Wan Wei implemented a desirability function based on artificial neural network for optimizing biohydrogen production process.[60] Kalogirou S. A. developed an artificial neural network model to optimize a solar-energy system in order to maximize its economic benefits.[61] In Wang Jiangfeng et al. study, an ANN model with the multi-layer feed-forward network is used to optimize the thermodynamic parameters for supercritical CO_2 power cycle with energy efficiency as objective function.[62] To date, there has been no previous studies in which ANN and RNN models were developed and used to explore the optimal steady state and dynamic operation of a pilot entrained flow gasifier in an IGCC plant; hence the novelty of the research considered in this study. Given the relevance of neural networks for this study, a general description of these methods is provided next.

2.3 Artificial Neural Networks

An artificial neural network consists of several layers of simple computing nodes, referred to as neurons, which predict different aspects of the input-output parameter relationship using nonlinear summing techniques. These layers typically consist of a number of hidden layers, as well as an

output layer. The hidden layer of the ANN determines the relationship between the inputs and the outputs, and the values calculated by hidden layer neurons are subsequently fed to the next layer. In the output layer, a linear transfer function maps the hidden layer outputs onto the range of the desired output parameters. The neurons in each layer of the ANN are interconnected via a series of weighted connection lines, as illustrated in Figure 3.

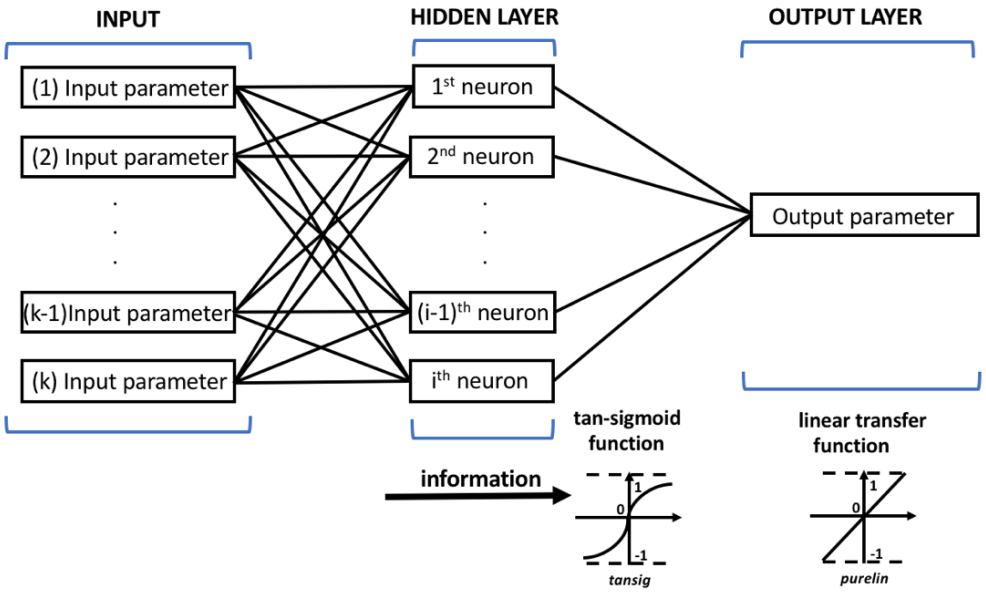

Figure 3. Brief configuration of artificial neural network

Each neuron consists of a weighted linear function and a transfer function, as denoted in Figure 4. There are mainly three types of transfer function (activation function) using in hidden layer, which are step-like functions, sigmoidal transfer functions and radial basis functions. The step-like functions are kind of threshold function and the networks with such neurons of step-like functions in hidden layer divide the input space into polyhedral areas. However, the step-like functions have discontinuous derivatives, preventing the use of gradient-based error minimization training procedures. Sigmoidal transfer functions allow to define popular continuous graded

response neurons and it is widely used in neural networks for regression. Radial basis functions are always used in pattern recognition problems.[63]

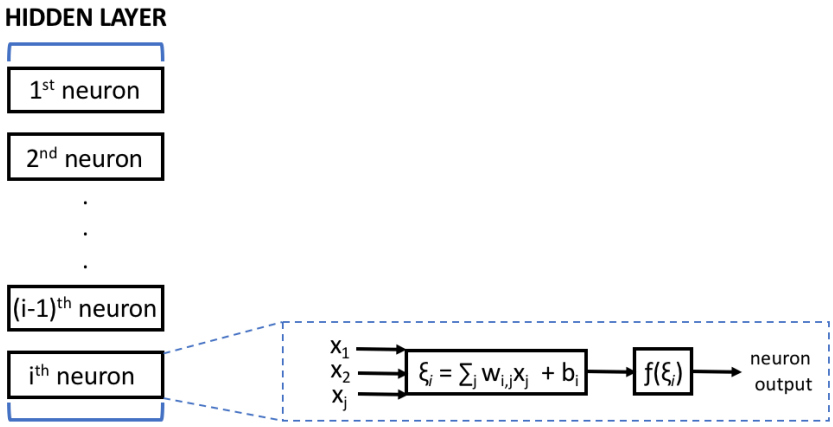

Figure 4. The structure of a neuron and its activation function

As shown in Figure 4, ξ_i denotes the linear weights function for the i^{th} neuron, which is defined as the sum of each of the j^{th} outputs from the previous layer (input layer); whereas x_j denote the input value of the j^{th} input parameter from the j^{th} neuron in the input layer, and the terms $w_{i,j}$ and b_i in ξ_i denote the weight and bias values applied to the i^{th} neuron, respectively. Furthermore, the function f denotes the transfer function applied to ξ_i. The transfer function applied in the hidden layers of an ANN usually consists of a sigmoidal function that maps ξ_i onto a nonlinear curve, whereas a linear transfer function is typically applied to the output layer to map ξ_i onto the range of the output parameters.

In order for the artificial neural network to function properly, it is necessary to adjust the weights and the biases of each neuron such that the artificial neural network can predict the output results for a given set of input parameters. This can be accomplished through supervised training, in which the network is provided with a series of input parameters and their corresponding output values. Training supervised networks requires a measure of the discrepancy between the network

and target outputs; the difference between these values yields an error function, often referred to as the network performance, which is defined as follows:

$$J(\mathbf{w}, \mathbf{b}) = \frac{1}{n}\sum_{i=1}^{n}\left(h_{w,b}\left(x^{(i)}\right) - y^{(i)}\right)^2 \quad (1)$$

where $J(\mathbf{w}, \mathbf{b})$ denotes the objective function of the training process; $\mathbf{w}$ and $\mathbf{b}$ denote the vector of weights and biases that will be optimized over the course of the training process. Furthermore, the symbol n represents the number of data pairs used to train the network, whereas $x^{(i)}$ and $y^{(i)}$ denote the i^{th} inputs and target outputs of the artificial neural network, respectively, and $h_{w,b}$ represents the hypothesis nonlinear function defined such that $h_{w,b}\left(x^{(i)}\right)$ denotes the output values predicted by the artificial neural network.

At the beginning of the network training, each of the weights and biases ($w_{i,j}$ and b_i) are randomly generated from a uniform distribution within the active range of the tangent sigmoid transfer function and their values are subsequently updated via backpropagation (BP). In the classical BP algorithms, the network is trained using gradient descent where in the partial derivative of the performance is calculated with respect to $w_{i,j}$ and b_i. These gradients are subsequently used to update the weights and biases as follows:

$$w_{i,j} = w_{i,j} - \alpha\frac{\partial}{\partial w_{i,j}}J(\mathbf{w}, \mathbf{b}) \quad (2)$$

$$b_i = b_i - \alpha\frac{\partial}{\partial b_i}J(\mathbf{w}, \mathbf{b}) \quad (3)$$

where α denotes the network learning rate, which determines the size of step changes during each iteration of the training process. At the beginning of the network training, the derivatives of the objective function, and thus the changes in the weights and biases, are large with respect to the network inputs. As the learning progresses, however, the derivative values and the values of $w_{i,j}$ and b_i stabilize as the network approaches a local minimum on the error surface.

In order to avoid overfitting in the neural network model, it is necessary to analyze the ANN performance during training in order to prevent the network from simply memorizing the training data. For the ANN training algorithm implemented in this work, an early stopping method was utilized, which partitions the input-output dataset provided into three parts: the training set, the validation set, and the testing set. During network training, the training set is used to optimize the weights and biases of each neuron so as to minimize the error between the ANN model outputs and the training data outputs. After each epoch of training, the network is fed with the input data from the validation set and used to predict the network output under these conditions. These predicted outputs are subsequently compared to the validation data outputs in order to calculate the validation error. The network is then subsequently re-trained for another epoch using the training dataset. This process continues until the validation error is either sufficiently small or it doesn't significantly change after a certain number of successive epochs.[64] After the training has been completed, the testing dataset is used to validate the performance of the ANN model. If the testing error obtained from this process is insufficiently small, then the input-output data is redistributed between three datasets and the network is retrained until the errors meet the user-defined criterion.[45]

2.4 Summary

In this chapter, a review of relevant studies on diverse modeling approaches on the gasification unit in IGCC system is presented. In the first part, a brief description of IGCC power plant and the gasification process in IGCC was provided with the aim to explain the key role of the gasifier in IGCC, and the need to model the steady state behaviour and transient performance of this unit. In order to conduct optimization on operating conditions of gasifier, the development of computationally efficient models that can capture key features of the gasifier is essential to assess

the behaviour of a gasifier. Subsequently, in the second part, CFD model, ROM and artificial neural network model on energy systems were reviewed. The limitations in using CFD models and ROM simulations are explained since computational cost of these two models are much higher compared with ANN models. Since the ANN models have low computational time, they are suitable to perform optimization on steady state and transient behaviour of the gasifier. The next chapter presents the development of ANN model for CanmetENERGY's pilot-scale gasifier, and the steady-state optimization of this pilot entrained-flow gasifier.

Chapter 3
Modelling and Optimization of a Pilot-scale Entrained-Flow Gasifier using Artificial Neural Networks

This chapter presents the construction of an artificial neural network (ANN) of a pilot-scale gasifier unit, which was trained using data generated for a large set of randomly-generated input conditions from a pilot-scale gasifier reduced order model (ROM) previously developed in our research group. Section 3.1 briefly introduces the reduced order model (ROM) of the pilot-scale gasifier considered in this study. Section 3.2 presents the validation of the fully-trained ANN via comparing its performance to the gasifier's ROM model. Section 3.3 presents the optimization studies proposed in this work using the validated ANN model. The scenarios considered in this study were aimed to determine the operating conditions that would maximize carbon conversion and the optimal conditions that would maximize both carbon conversion and production of hydrogen gas, which are two conflicting objectives. Note that most of the contents of this chapter has been already published in a journal.[42]

3.1 Introduction of ROM for a pilot-scale gasifier

The entrained-flow IGCC gasifier system modeled in this work consists of a tonne-per-day (TPD) pilot-scale gasifier owned by CanmetENERGY, Natural Resources Canada, which is briefly illustrated in Figure 2.[26] This pilot gasifier is lined with refractory and insulation materials in order to reduce its heat loss, as it has a large surface area to volume ratio. Fuel, steam (H_2O), oxygen (O_2) and nitrogen (N_2) are fed into the gasifier to produce raw syngas. The pet-coke's temperature often ranges from 270 K to 330 K before it is loaded into the gasifier, as the initial temperature significantly affects the gasifier temperature profile when the fuel is mixing with the steam. In addition, the composition of the pet-coke in the fuel (i.e., the mass fraction of ash, volatiles, and

moisture) plays a crucial role in the reaction process and the formation of the volatile products.

As mentioned above, IGCC gasifier models are conventionally modelled using CFD models[65,66,8], which can provide an accurate and detailed outlook for the gasification system but they can be extremely computationally expensive. This has motivated the development of more efficient modelling methods such as reduced order models (ROMs). These ROMs are an alternative approach that can be used to provide detailed information about the multi-phase flow structure of a gasification unit such as its solid particle concentration, composition, and temperature distribution along the length of the gasifier.

Sahraei et al.[13] proposed a reactor network ROM consisting of different plug flow reactor (PFR) and continuous stirred tank reactor (CSTR) models to simulate each of the different zones at steady state inside the entrained-flow gasifier mentioned above. The key input parameters of the ROM are inlet flow rate of pet-coke, steam, oxygen and nitrogen, the initial temperature of the pet-coke, and the percent composition of ash, volatiles, and moisture within the pet-coke. The pet-coke composition contained a molar fraction of 0.046 ash, 0.127 volatiles, and 0.005 moisture and 0.822 carbon. The ROM was developed over an explicit input parameter range determined experimentally on the pilot-scale gasifier, and consequently the ROM is only valid for this specific range of operating conditions.

The performance of a gasifier can be described by the conversion of its reactants, the concentration of its desired products at the outlet, and the temperature distribution throughout the unit.[25] In the ROM model, the carbon conversion is the main important output parameter for characterizing the gasifier performance, as it serves to measure the fraction of solid coal converted into the more useful syngas form. In addition, the gasifier products, i.e., CO and H_2, provide a much lower heating value and require lower operating temperatures, and thus they are able to achieve much greater efficiency than their solid fuel alternatives. Consequently, it is important to be able to predict the molar percentage of CO and H_2 in the outlet gas flow as a

function of the input parameters. Another significant observable of the gasifier system is the internal temperature, which has a significant effect on the reactions taking place. Specifically, the peak temperature of the gasifier are monitored in order to keep it below the maximum temperature that the refractory brick layer within the gasifier can bear.[25] Furthermore, standard measurement devices such as thermocouples are often used in industrial reactors to monitor the temperature at key locations inside the unit. For the specific IGCC gasifier unit considered in the ROMs model work, there are four thermocouples located on the wall of the gasifier reactor, so that the operations can observe and monitor the temperature distribution at these discrete locations. The location of each thermocouple is detailed in Figure 2.

The ROM reactor network considered in this work decomposes the gasifier system into three different types of zones referred to as the jet expansion zone (JEZ), external recirculation zone (ERZ), and down-stream zone (DSZ) regions, as outlined in the Figure 5.

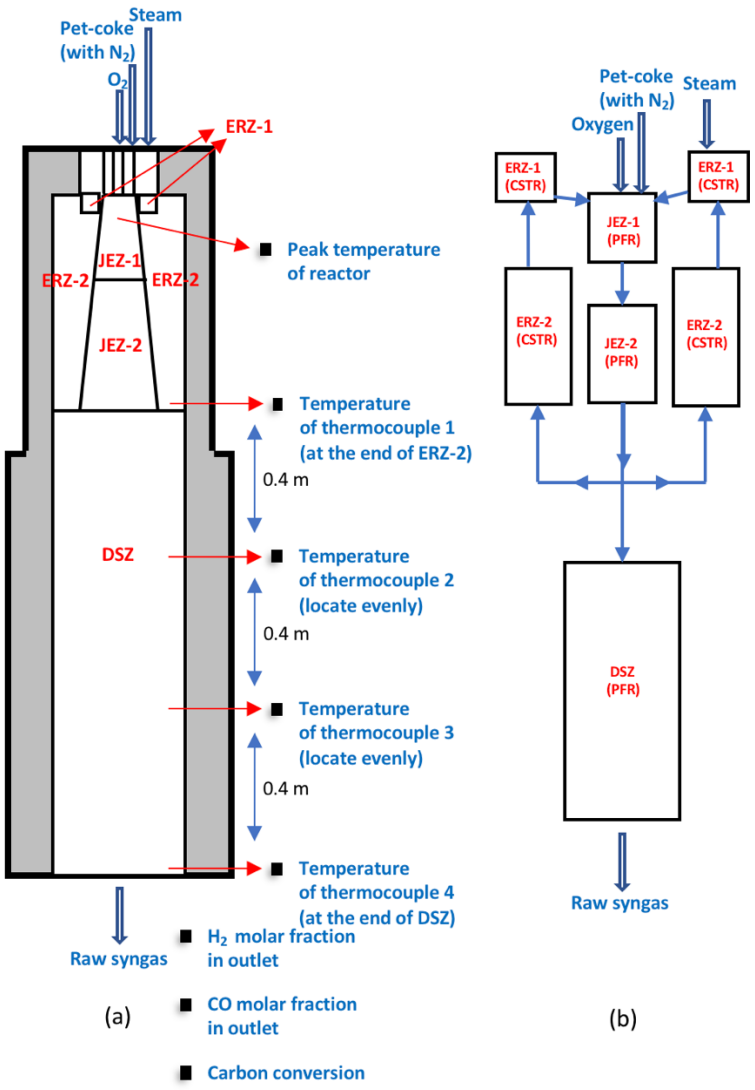

Figure 5. (a) Reactor network of the gasifier; (b) Corresponding regions of the reactor network inside the gasifier

As shown in Figure 5, the JEZ and DSZ are modeled as plug flow reactors (PFRs) whereas the ERZ zones are modeled as continuous stirred tank reactors (CSTRs). Rather than solving the differential equations across the entire gasifier domain using CFD techniques, the ROM reduces the order of equations inside each gasifier zone, e.g., ERZ zones can be considered as a single node because of uniform particle and temperature distributions. In the JEZ region, the steam, and oxygen are suddenly expanded at the gasifier inlet, which causes the flow of fuel to spread out.

When the flow reaches the gasifier wall, a portion of the stream recycles back to the top of the gasifier through the ERZ region while the rest of the stream flows towards the DSZ region at the bottom of the reactor. Inside each reaction zone, the gasifier's behaviour is simulated based on the flow characteristics (i.e., whether they are mixed or laminar) and the one-dimensional governing equations of gas and solid phases for mass, energy, and momentum are solved for each zone to provide a distribution of different properties. The conservation equations of mass, energy and momentum used to simulate each zone of the gasifier are listed in Table 2 (see the Nomenclature section for the definition of the model parameters).

Table 2. Mathematical model of the multi-phase flow in the ROM[12]

Gas phase	
Momentum	$-\frac{\partial(\mathrm{A}_{cs}\varepsilon_{\mathrm{g}}\rho_{\mathrm{g}}u_{\mathrm{g}}^2)}{\partial \mathrm{x}}+\mathrm{A}_{cs}(-\frac{dP}{dz}+\varepsilon_{\mathrm{g}}\rho_{\mathrm{g}}\mathrm{g}-F'_{\mathrm{g},w}-F'_{\mathrm{g},p})=0$
Mass	$\frac{\partial}{\partial \mathrm{x}}\left(\mathrm{A}_{cs}D_{\mathrm{g,eff}}\frac{\partial(\varepsilon_{\mathrm{g}}\mathrm{C}_{\mathrm{g}_i})}{\partial x}\right)-\frac{\partial\left(\mathrm{A}_{cs}\varepsilon_{\mathrm{g}}u_{\mathrm{g}}\mathrm{C}_{\mathrm{g}_i}\right)}{\partial \mathrm{x}}+\mathrm{A}_{cs}\left(\mathrm{MS}_{\mathrm{g}_i}^{\mathrm{Hetero}}+\mathrm{MS}_{\mathrm{g}_i}^{\mathrm{Homo}}\right)=0$
Energy	$\left(\mathrm{A}_{cs}k_{\mathrm{g,eff}}\frac{\partial T_g}{\partial \mathrm{x}}\right)-\frac{\partial\left(\mathrm{A}_{cs}\varepsilon_{\mathrm{g}}u_{\mathrm{g}}\mathrm{C}_{\mathrm{g}_{\mathrm{total}}}c_{\mathrm{p}_{\mathrm{g}}}T_{\mathrm{g}}\right)}{\partial \mathrm{x}}+\mathrm{A}_{cs}\left(\varepsilon_{\mathrm{g}}\mathrm{HS}^{\mathrm{Hetero}}+\mathrm{HS}_{\mathrm{g}}^{\mathrm{Homo}}\right)+\mathrm{Q}'_{\mathrm{conv\,g\to p}}-\mathrm{Q}'_{\mathrm{conv\,g\to w}}-\mathrm{Q}'_{\mathrm{w\to s}}=0$
Solid phase	
Momentum	$-\frac{\partial}{\partial \mathrm{x}}\left(\mathrm{A}_{cs}\varepsilon_p\rho_p u_p^2\right)+\mathrm{A}_{cs}\left(\varepsilon_p\rho_p\mathrm{g}+F'_{\mathrm{g},p}\right)=0$
Mass	$-\frac{\partial\left(\mathrm{A}_{cs}\varepsilon_p u_p C_p\right)}{\partial \mathrm{x}}+\mathrm{A}_{cs}\left(\mathrm{MS}_{\mathrm{p}}^{\mathrm{Homo}}\right)-\mathrm{m}'_{\mathrm{slagging}}=0$
Energy	$-\frac{\partial}{\partial \mathrm{x}}\left(\mathrm{A}_{cs}\varepsilon_p u_p C_p c_{p_p}T_p\right)+\mathrm{A}_{cs}\left(\varepsilon_{\mathrm{p}}\mathrm{HS}^{\mathrm{Hetero}}\right)-\mathrm{Q}'_{\mathrm{conv\,p\to g}}-\mathrm{Q}'_{\mathrm{rad\,p\to w}}-\mathrm{m}'_{\mathrm{slagging}}\mathrm{h}_{\mathrm{p}}=0$
Number of particles	$\frac{\partial(\mathrm{A}_{cs}\mathrm{N}_{\mathrm{p}}u_p)}{\partial \mathrm{x}}+\frac{\mathrm{m}'_{\mathrm{slagging}}}{\mathrm{m}_{\mathrm{p}}}=0$

As indicated in previous studies, the ROM used in this work was validated using both CFD simulation results[12] and experimental data[12] obtained from CanmetENERGY's pilot-scale gasifier. A more detailed model description of the ROM as well as the descriptions for the model parameters presented in this table can be found elsewhere in the literature.[12] However, it is important to note that even though the ROMs require substantially lower computational costs compared to CFD models, they still require considerable numerical analysis and thus they are still computationally expensive for optimization, monitoring and online control applications.

3.2 Development of ANN model for a pilot-scale gasifier

In this work, an artificial neural network was developed to calculate the key outputs of the pilot-scale gasification unit such as the carbon conversion, outlet composition, peak temperature, and temperature at the thermocouples' location, as a function of the relevant system parameters, such as the inlet gas flowrates, the inlet temperature, and the fuel composition. The developed ANN consisted of a number of sub-ANNs that were each developed to predict the performance of each output parameter individually as a function of the inputs. The sub-ANNs were developed using a two-layer neural network structure that consisted of a single hidden layer with a tan-sigmoid transfer function and an output layer with a linear transfer function, as illustrated in Figure 3. Note that the two-layer neural network structure was selected as the basis for the ANN as it is considered to be the most suitable structure for nonlinear model fitting regression problems.[67] Furthermore, no significant performance improvements were observed when the number of layers in the ANN sub-networks were increased. Each ANN was trained using data obtained from the ROM reported previously in Section 3.1.[13] The following sections will provide a brief overview of the ANN methodology implemented in this work. A general overview of the feedforward ANN structure and its backpropagation algorithm is provided, followed by a brief description of the

gasifier variables that serve as the input and output parameters to the ANNs. Subsequently, the performance of various back-propagation algorithms on the ANN training are compared, and the optimal number of hidden layer neurons are determined for each ANN in order to optimize their predictive capabilities.

3.2.1 Input and output training data

The carbon conversion (T_1), the molar composition of CO (T_2) and H_2 (T_3), peak temperature of the gasifier (T_4), and the temperature at the four thermocouples located on the wall of the gasifier reactor (i.e., T_5 - T_8), all serve as the desired measurable outputs for the gasifier system, and thus are considered as the key output parameters (***T***) to be predicted using the ANN model. On the other hand, the key input parameters (***P***) that affect the gasifier performance are the injected fuel flowrate (P_1), the oxygen flowrate (P_2), the nitrogen flowrate (P_3), the steam flowrate (P_4), the initial fuel temperature (P_5), and the fuel compositions of ash (P_6), volatiles (P_7), and moisture (P_8). Consequently, these parameters serve as the inputs which the ANN model would use to predict the desired outputs. More information about each of these input and output parameters can be found in Section 3.1. Furthermore, Table 3 provides a comprehensive list of the input (***P***) and output (***T***) parameters, their nominal values, and the corresponding minimum and maximum input parameter values over which the ANN was trained. These input ranges were determined experimentally using the ROM in order to guarantee that they are feasible and capable of obtaining reasonable results for both the ROM and ANN models. Note that the fuel composition parameters (P_6, P_7, & P_8) cannot be accurately controlled, as the fuel composition can only be coarsely altered by changing the type of coal used. Consequently, the ranges for these parameters were determined by applying a $\pm$5% fluctuation around the expected values for each fuel component, as this was determined to provide satisfactory composition bounds via laboratory experiments.[12]

Table 3. Key gasifier input and output parameters

Input parameters (***P***)	Nominal condition ($\boldsymbol{P}_{nom}$)	Lower bound ($\boldsymbol{P}_{min}$)	Upper bound ($\boldsymbol{P}_{max}$)
P_1: Fuel flowrate (kg/h)	41.2	41.2	52.3
P_2: O_2 flowrate (kg/h)	37.2	28.4	37.2
P_3: N_2 flowrate (kg/h)	12.1	11.0	12.1
P_4: Steam flowrate (kg/h)	10.7	0	21.8
P_5: Fuel temperature (K)	300	270	330
P_6: Mass fraction of ash in fuel	0.046	0.0414	0.0506
P_7: Mass fraction of volatiles in fuel	0.127	0.1143	0.1397
P_8: Mass fraction of moisture in fuel	0.005	0.0045	0.0055

Output parameters (***T***)	Output values at nominal condition
T_1: Conversion	0.9134
T_2: Outlet CO composition	0.5135
T_3: Outlet H_2 composition	0.2176
T_4: Peak temperature (K)	2.6631×10^3
T_5: Temperature: Thermocouple 1 (K)	1.9114×10^3
T_6: Temperature: Thermocouple 2 (K)	1.7864×10^3
T_7: Temperature: Thermocouple 3 (K)	1.6726×10^3
T_8: Temperature: Thermocouple 4 (K)	1.6090×10^3

In order to train the ANN model, it is necessary to generate a large number of data points for each model output using various combinations of each of the input parameters. For the study presented in this work, the ANN data was generated using 8,000 combinations of input parameters randomly generated from a uniform distribution, between their upper and lower bounds as listed in Table 3. Trial-and-error simulations were performed to determine a suitable data set for the identification

of the ANNs. Increasing the sample size beyond 8,000 samples increases the computational effort but it does not improve the prediction capabilities of the ANNs. Each of these input parameter combinations were passed through the ROM in order to determine their corresponding output parameter values; these input and output parameters were subsequently paired up and fed into the training process used to generate the ANNs model.

3.2.2 Selection of back-propagation algorithm

The backpropagation method is one of the most crucial concepts for enabling the self-learning capabilities of an ANN.[68] This methodology refers to the ability of a neural network to adjust the values of its weights and biases based on the error in the network outputs.[69] As a result, it is important to select a good back-propagation method to ensure that the network can accurately and efficiently learn to predict the outputs of a system given a set of inputs without being subject to overfitting. In this study, we compared eight different BP algorithms with the aim of choosing the best fitting algorithm for the gasifier data collected. Each BP algorithm considered is not discussed within this paper for the sake of brevity; further discussion about these algorithms can be found within the literature.[70,71] Each BP algorithm was used to train a two-layer ANN with 10 neurons in the hidden layer in order to predict the outlet CO composition (T_2) as a function of each of the input parameters $\boldsymbol{P}$.

The results of the network training for each BP algorithm are presented in Table 4. These results reveal that the Levenberg-Marquardt algorithm is the best BP algorithm for the ANN system considered in this work, as it managed to achieve the lowest mean squared training error with a minimum value of 2.30×10^{-7}. Furthermore, the training was stopped after 138 epochs. Even though the Scaled conjugate gradient and One-step secant BP can achieve the similar error magnitude and R value to the Levenberg-Marquardt algorithm, both of them needed more training

iterations which means that they required more time to obtain the optimal weights and bias of their corresponding ANN models. The weakest BP training algorithms are Gradient descent with momentum and Gradient descent, which needed the most iteration numbers to find the optimal weights and bias and produced the largest magnitude of mean squared errors of the trained ANN models.

Table 4. Comparison of the backpropagation algorithms

BP algorithm	R values	Mean squared error	Iteration number
Levenberg-Marquardt	0.999	2.30×10^{-7}	138
Scaled conjugate gradient	0.999	6.36×10^{-7}	363
One-step secant BP	0.999	3.71×10^{-7}	349
BFGS Quasi-Newton	0.996	1.12×10^{-5}	128
Gradient descent with momentum and adaptive LR	0.998	1.85×10^{-4}	227
Gradient descent with momentum	0.980	0.0178	1,000
Resilient backpropagation	0.999	1.70×10^{-6}	600
Gradient descent	0.998	0.0155	1,000

These results are further validated in Figure 6 which showcases the training and validation mean square errors at each epoch of the network training using the Levenberg-Marquardt algorithm. This figure additionally illustrates that the network training results were reasonable, as the train and validation errors both displayed similar characteristics, and these two errors did not change significantly upon further training. As shown in Figure 6, the validation error reached the minimum

best validation mean squared error (MSE), when MSE of validation does not decrease for six consecutive epochs. As a result, the Levenberg-Marquardt algorithm was implemented to train the ANN model developed in this work.

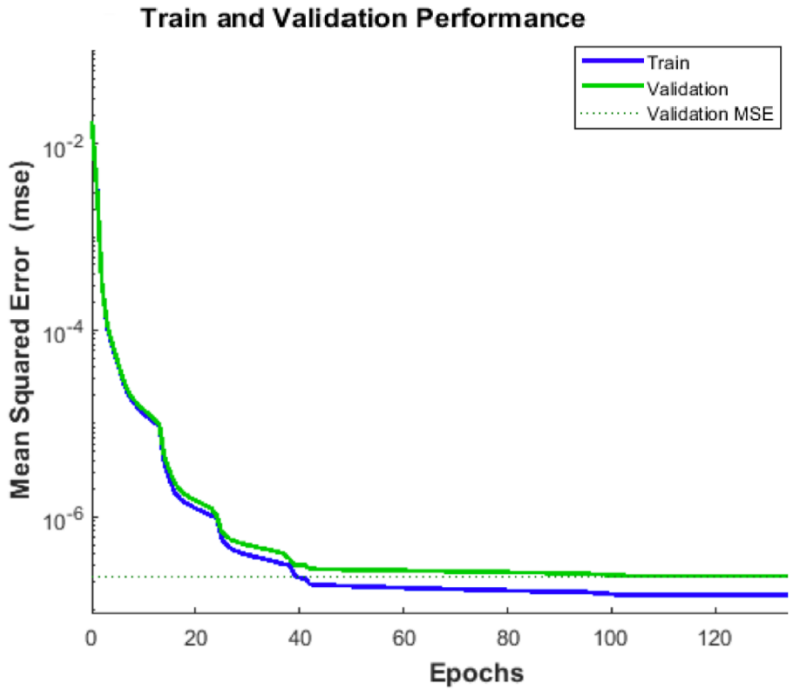

Figure 6. Mean square errors obtained during training, validation, and testing, using the Levenberg-Marquardt algorithm

3.2.3 Neural network structure

The aim of this section is to perform optimization on the number of hidden layer neurons for each of the eight sub-ANNs developed in this work to predict each gasifier output. Each sub-network was developed using the two-layer architecture described previously, using the Levenberg-Marquardt algorithm for back-propagation. In this study, each sub-network was initialized with a hidden layer containing only a single neuron, and the sub-networks were trained to predict each of the model outputs as a function of the inputs. Subsequently, the number of neurons in each

hidden layer was incremented by one and the networks were re-trained using the same data. This data was used to calculate the mean squared validation and testing errors for each network as a function of the number of hidden layer neurons. This process was repeated until the sub-network was observed to be memorizing the data, (i.e., when sub-network's validation error decreased but its testing error was observed to increase), at which point the optimization process was terminated for that network.

The results of the identification of the optimal structure for each of the ANN developed in this work are shown in Table 5. The normalized mean squared error (MSE) for the eight output parameters (T_1 - T_8) is less than 5×10^{-5}. This model fitting was achieved by adjusting the number of neurons in hidden layer. Furthermore, the maximum percentage error between the actual output obtained by the trained ANN and the target output generated by the ROM for test and validation sets in the training process are sufficiently low, i.e. less than 3% for all the output parameters except for the temperature at thermocouple 1 (T_5). Although the maximum percentage error in the temperature at thermocouple 1 (T_5) is 6.0% and 5.24% for test set and validation set respectively, they are still in reasonable agreement with the ROM data. Noted that the maximum percentage error between the test and validation set are similar to each other for each output parameter, which is an indication that there is no overfitting in each ANN model.

Table 5. The optimal number of hidden layer neurons, and resulting testing and validation errors, for each output parameter captured by the ANN

Output parameters	Neuron number	Normalized MSE		Maximum percentage error	
		test	validation	test	validation
Conversion (T_1)	5	2.7559×10^{-5}	3.7119×10^{-5}	2.5641%	2.6741%
CO composition (T_2)	4	1.9744×10^{-5}	2.0141×10^{-5}	1.2188%	1.5834%
H2 composition (T_3)	3	2.0877×10^{-5}	2.3952×10^{-5}	2.2514%	1.7657%
Peak temperature (T_4)	5	2.8234×10^{-5}	3.2510×10^{-5}	2.4972%	2.2134%
Thermocouple 1 (T_5)	6	1.9301×10^{-5}	1.5632×10^{-5}	6.0075%	5.2366%
Thermocouple 2 (T_6)	6	1.8556×10^{-5}	1.8901×10^{-5}	2.9233%	2.5796%
Thermocouple 3 (T_7)	6	2.6874×10^{-5}	1.6053×10^{-5}	1.5751%	1.4401%
Thermocouple 4 (T_8)	6	3.7088×10^{-5}	2.2285×10^{-5}	0.7688%	1.2136%

Figure 7 illustrates the optimal neural network structure for each of the sub-networks and provides the general framework of the ANN model considered in this study.

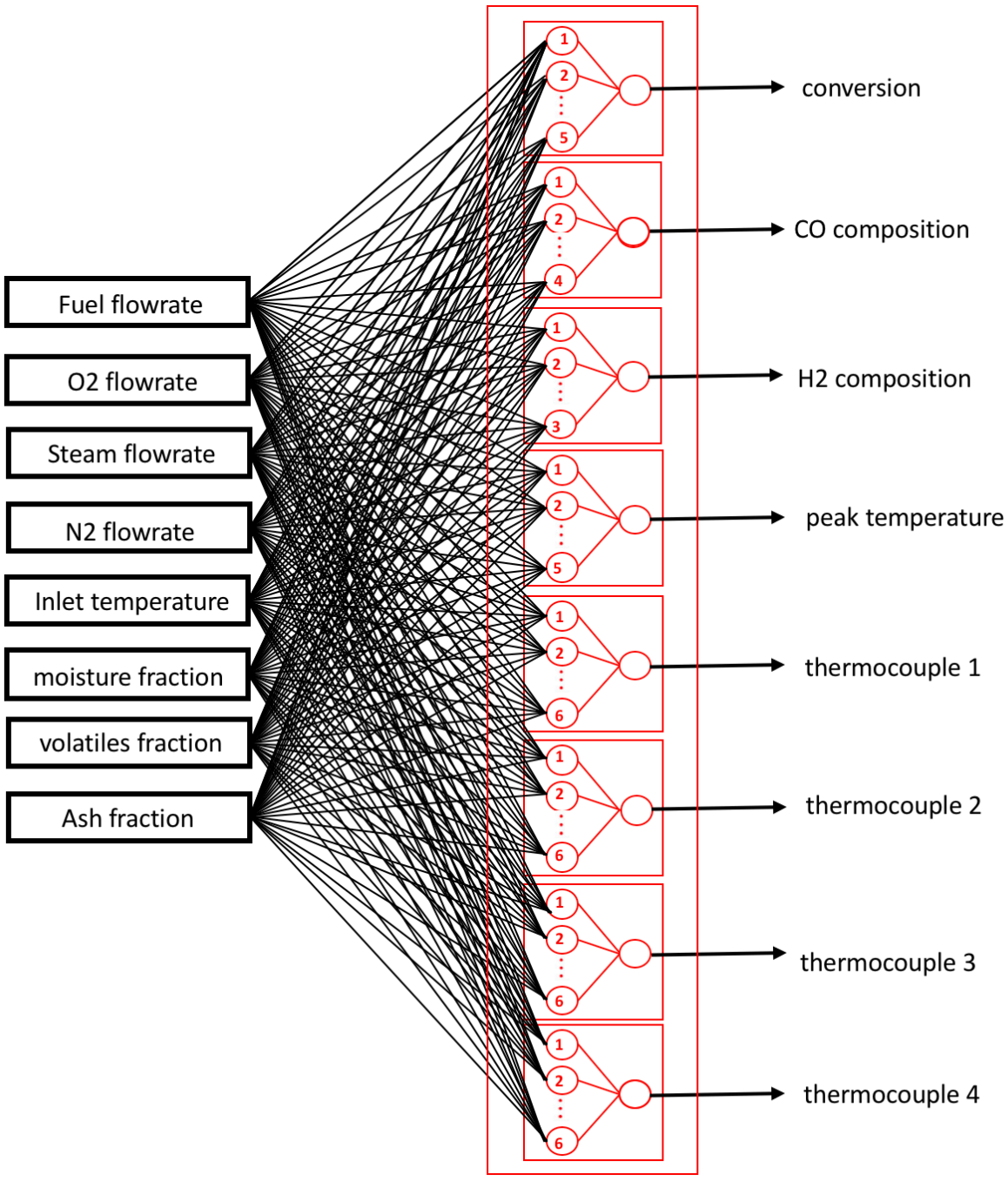

Figure 7. Optimal neural network structure for the IGCC pilot-scale gasifier

Furthermore, Figure 8 showcases the linear regression analysis between the ANN outputs generated using the optimal number of hidden neurons and the corresponding output targets for T_2, the molar fraction of CO at the outlet. As can be seen by these results, the ANN can adequately predict the target output data given the non-linear relationship between the inputs and outputs for the output parameter (T_2). A similar performance was observed for the rest of the output parameters but it is not shown here for brevity.

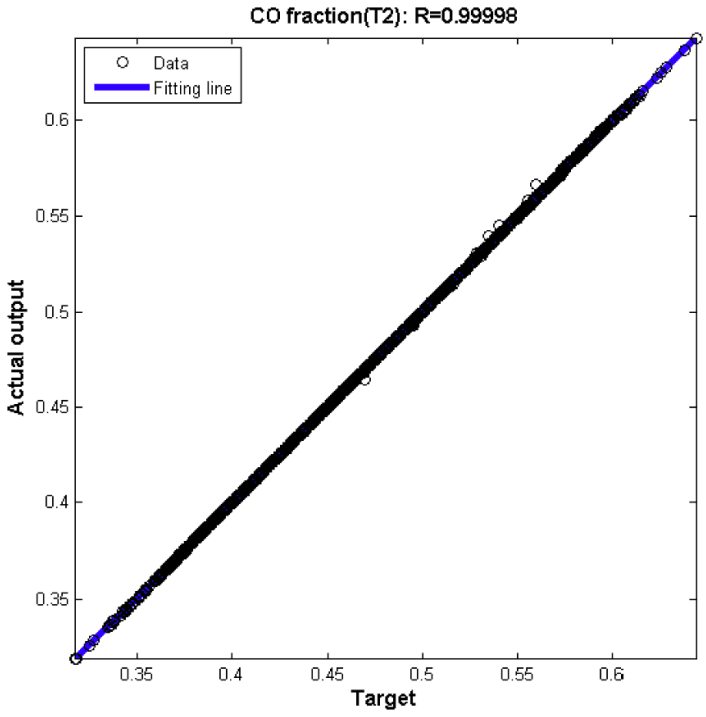

Figure 8. Regression between network output values and target output values for T_1

3.3 ANN model validation

The objective of this section is to test and validate the performance of the ANN model described previously in Section 3.2. The ANN's performance was evaluated with respect to the ROM which has been reported previously in the literature.[24] Note that the accuracy of the ANN is dependent

on the predictive capabilities achieved via the training process described in Section 3.2. Therefore, the ANN output performance was validated subject to changes in each of the input parameters ***P*** listed in Table 3. In order to ensure good generalization for each ANN model, the trained ANN model was tested using 2,500 combinations of input parameter values that had not been previously used during the network training. As a result, each combination of the eight input parameters utilized in this study was generated afresh via random selection from a uniform distribution within the parameter ranges showcased in Table 3, i.e., the parameter ranges over which the networks were trained. Each of these combinations were inspected *a priori* in order to ensure that they were different from the data used to train the ANN model and its sub-networks. Table 6 presents 10 out of the 2,500 combinations of input parameters used to validate the performance of the ANN. The performance of both the ROM and ANN models for these ten combinations of input parameters, as assessed through each of the eight output parameters, are illustrated in Figure 9. Note that the outputs for the remaining 2,490 sample points used for model validation are not shown here for the sake of brevity; however, their results were comparable to those illustrated in Figure 9. In addition, Table 6 displays the sum of squared errors of the outputs between the results of the ROM and the ANN model for the full batch of 2,500 input operating condition combinations. These results show that the ANN model is able to adequately capture the behavior of the gasifier unit, and that the ANN model is not overfitting. As shown in Figure 9, the profile of each eight outputs determined using the ROM match those determined using each of the ANN sub-networks.

Table 6. First ten combination of input parameters used to validate the ANN

Input parameter	1	2	3	4	5	6	7	8	9	10
P_1 (Fuel flowrate, kg/h)	44.93	48.19	50.80	43.67	45.42	43.60	46.11	46.68	49.68	42.90
P_2 (O_2 flowrate, kg/h)	35.48	34.31	32.08	31.57	29.40	29.18	30.06	36.48	35.22	35.87
P_3 (N_2 flowrate, kg/h)	11.40	11.63	11.37	11.28	11.62	11.89	12.02	11.91	11.99	11.63
P_4 (Steam flowrate, kg/h)	20.46	0.12	20.99	18.05	16.46	16.39	3.92	6.72	20.42	6.01
P_5 (Fuel temperature, K)	280.24	277.59	324.90	313.38	309.90	319.86	306.71	287.15	272.94	321.78
P_6 (Mass fraction of ash)	0.0466	0.0484	0.0469	0.0452	0.0498	0.0429	0.0428	0.0470	0.0490	0.0449
P_7 (Mass fraction of volatiles)	0.1389	0.1346	0.1392	0.1376	0.1277	0.1390	0.1210	0.1272	0.1267	0.1269
P_8 (Mass fraction of moisture)	0.0046	0.0048	0.0048	0.0051	0.0047	0.0050	0.0054	0.0047	0.0049	0.0050

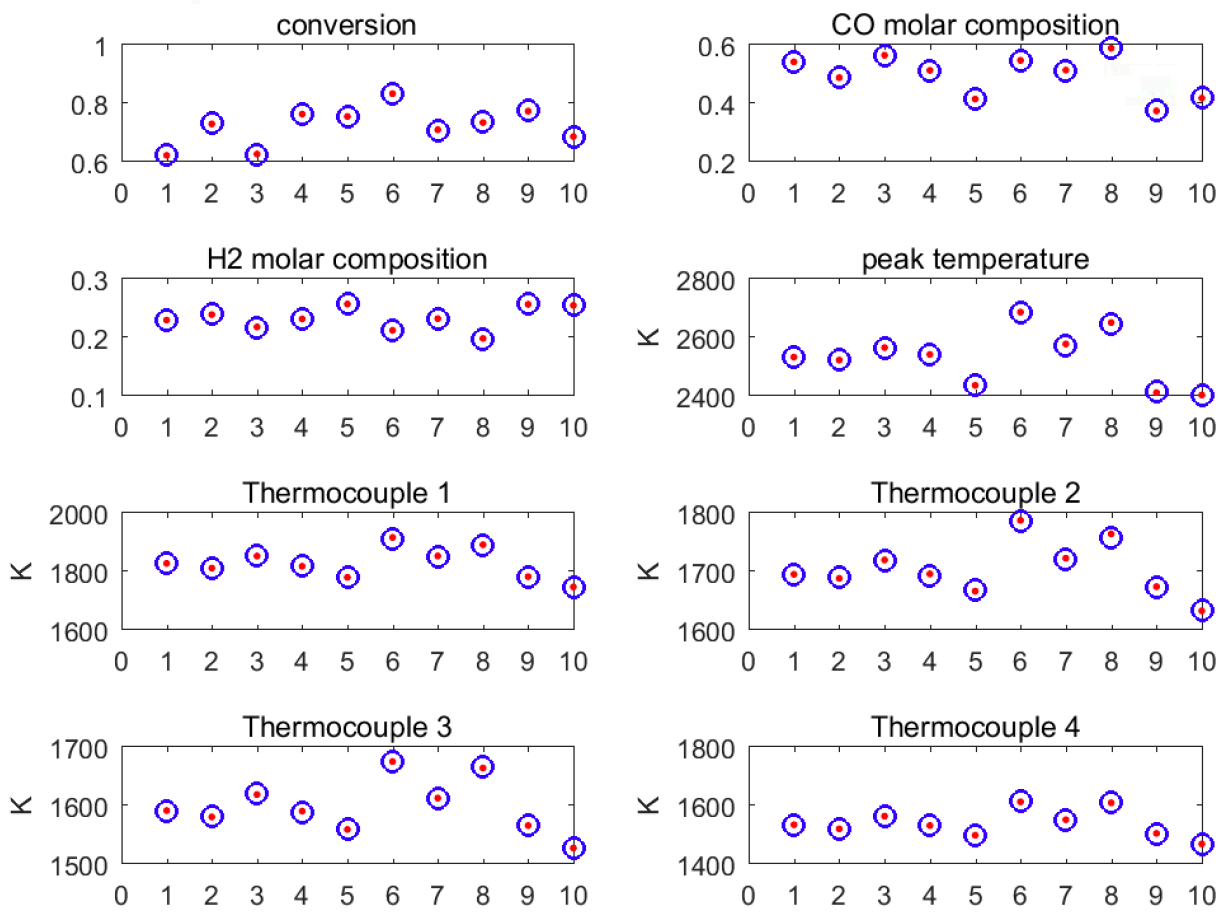

Figure 9. Comparison of the gasifier outputs obtained for the first ten combinations of input validation data as generated by the ANN model (represented as blue circles) and the ROM (represented as red dots)

Furthermore, Table 7 shows that the errors in the ANN-predicted outputs remain sufficiently low, i.e., $< 2.5 \times 10^{-3}$ and $< 6 \times 10^{-2}$ for the mean and maximum relative errors respectively for all eight output parameters. Note that the sum of squared errors for each of the temperatures (i.e., the peak temperature and the temperatures at the thermocouple locations), as shown in Table 7, are notably larger than the remaining output parameter errors; this is because the temperatures are of higher orders of magnitude compared to the other outputs, and thus they are subject to larger absolute errors. With regards to the computational cost, the ROM model and the ANN model

required on average about 257 s and 1.6×10^{-3} s of CPU time per simulation, respectively (Intel® Core™ i7-4770 CPU @ 3.40 Hz, 3392 Mhz, 4 Core(s), 8 Logical Processor(s)). This difference in the computational time illustrates that the ANN is approximately 1.6×10^{5} times faster than the ROM model. This demonstrates that the ANN is significantly more computationally efficient compared to the ROM, while achieving sufficiently similar results. Overall, this validation study demonstrates that the ANN model is able to predict the steady state behavior of the gasification reactor accurately and can be used to perform optimization studies.

Table 7. The mean squared, mean, and maximum errors obtained for all eight output parameters over 2,500 input combinations

Output parameters	MSE	Mean error	Max error
T_1 (Conversion)	4.7259×10^{-6}	0.2204%	2.5641%
T_2 (CO composition)	3.1658×10^{-7}	0.0662%	1.4744%
T_3 (H_2 composition)	4.2342×10^{-7}	0.2085%	1.5247%
T_4 (Peak temperature, K)	60.8380	0.1740%	2.1374%
T_5 (Thermocouple 1, K)	45.5503	0.1421%	5.3596%
T_6 (Thermocouple 2, K)	17.4942	0.1236%	2.8246%
T_7 (Thermocouple 3, K)	3.5040	0.0532%	1.7441%
T_8 (Thermocouple 4, K)	2.5240	0.0523%	1.0516%

3.4 Optimization: Carbon Conversion

Integrated Gasification Combined Cycle (IGCC) system using coal gasification is a crucial component of future energy alternatives. Since gasification is the most important component of this system, it is particularly critical to understanding the operation and optimizing the gasification unit.[72] In industrial applications, the performance of a gasification unit in an IGCC plant is characterized by its conversion of carbon (T_1) into gaseous products such as CO, CO_2 and CH_4; as a result, it is crucial to manufacture IGCCs that meet or exceed specific carbon conversion requirements in order to maximize the gasifier performance.[73,21] Note that the peak temperature of the gasifier reactor should be constrained to be within a reasonable range to avoid damaging the refractory wall due to the high temperature. For different gasifier reactor types, the material of the reactor wall would be different and therefore, the constraints of the peak temperature of gasifier can be adjusted so that they do not impose a safety hazard. Motivated by this, the first objective of this section is to optimize the gasifier carbon conversion at the reactor outlet under different peak temperature limitations using the ANN gasification model developed in Section 3.2. This optimization study was performed with respect to each of the input parameters $\boldsymbol{P}$ mentioned in Section 3.2.1 according to the following optimization formulation:

$$\max_{\boldsymbol{P}} T_1(\boldsymbol{P}) \tag{4}$$

Subject to:

$ANN\ model$

$T_4\ (\boldsymbol{P}) \leq T_{4,max}$

$\boldsymbol{P}_{min} \leq\ \boldsymbol{P} \leq \boldsymbol{P}_{max}$

where $\boldsymbol{P}_{min}$ and $\boldsymbol{P}_{max}$ represents the lower and the upper bounds for all the eight input parameters considered in $\boldsymbol{P}$, which can be found in Table 3. $T_{4,max}$ denotes the maximum allowable temperature that the refractory wall can bear, and the function of carbon conversion

(T_1) is a nonlinear function estimated by the ANN gasification model. The above optimization formulation was performed using different bounds of the peak temperature, i.e., $T_{4,max}$ was set to 2,400 K, 2,500 K, 2,600 K, and 2,700 K. This was done to obtain an insight to the effect of peak temperature limitation on the optimized results of carbon conversion and the remaining gasifier parameters. The results of the input parameters obtained from the different optimization runs were additionally fed into the ROM in order to validate the results of the ANN model, and the corresponding results of carbon conversion from ROM are similar to the optimized carbon conversion values run by ANN model. Then, these results from optimization by ANN were compared to the nominal reactor conversion predicted by the ROM using the nominal input values presented in Table 3.

The results of the optimization study are presented in Table 8. As can be seen by these results, the maximum carbon conversion increases correspondingly with the limitations of peak temperature rising. Notably, the maximum carbon conversion increases drastically from 0.8111 to 0.9702 when the limitation of peak temperature changes from 2,400 K to 2,600 K. While peak temperature limitation increases from 2,600 K to 2,700 K, the maximum carbon conversion does not increase notably (differences noted beyond five decimal digits). This result is consistent with the results obtained by ROM, as the percent error in the optimal carbon conversion between both modelling methods remain below 0.3% for the four different peak temperature limitation case studies considered here. At the nominal operating conditions ($\boldsymbol{P}_{nom}$) listed in Table 8, the ROM predicted a carbon conversion of 0.9134, which is about 5.85% lower than the value obtained from the present optimization case study (Case 3 & Case 4 in Table 8). Note that according to the results in Table 8, higher carbon conversions are associated with higher steam flow rates; thus, increasing the steam flow rates can promote higher carbon conversions. The results from the optimization also indicate that, as the maximum allowed peak temperature constraint is relaxed, the carbon conversion tends to increase significantly up until it reaches approximately

0.97 conversion, which seems to be the highest conversion that can be achieved for the nominal operation of the pilot-scale gasification unit considered in this study, when the limitation increase beyond $T_{4,max}$ = 2,600 K, the conversion does not tend to change significantly. Furthermore, the results also illustrate that a lower fuel flowrate, a higher steam flowrate, a higher inlet fuel temperature, and higher mass fraction of ash, volatiles and moisture would also lead to a higher carbon conversion. As a result, the optimization study predicts that higher ratios of steam and oxygen to pet-coke are required in order to obtain higher carbon conversions. Table 8 additionally shows that the optimization results obtained using the ANN are similar to the values obtained using the ROM, which demonstrates that the ANN is able to accurately predict the gasifier outputs for optimization applications. Each of the optimization runs required an averaged CPU time of 0.0808 s, however, the same optimization study using the ROM required 7,573 s; i.e., at least four orders of magnitude the time needed to perform the same optimization using the ANN.

Table 8. Carbon conversion optimization results

parameter name	Nominal condition	Case 1 ($T_{4,max}$ =2400K)	Case 2 ($T_{4,max}$ =2500K)	Case 3 ($T_{4,max}$ =2600K)	Case 4 ($T_{4,max}$ = 2700K)
P_1 (Fuel Flow Rate, kg/h)	41.2	40	40	40	40
P_2 (O_2 Flow Rate, kg/h)	37.2	30.8921	34.449	37.2	37.2
P_3 (N_2 Flow Rate, kg/h)	12.1	12.1	12.1	11	11
P_4 (Steam Flow Rate, kg/h)	10.7	21.8	21.8	19.2112	19.2111
P_5 (Fuel Temperature, K)	300	330	330	330	330
P_6 (Mass Fraction Ash)	0.046	0.0506	0.0506	0.0506	0.0506
P_7 (Mass Fraction Volatiles)	0.127	0.1397	0.1397	0.1397	0.1397
P_8 (Mass Fraction Moisture)	0.005	0.0055	0.0055	0.0055	0.0055
Optimized parameter					
T_1 (Conversion) in optimization using ANN		0.8111	0.9033	0.9702	0.9702
T_1 (Conversion) run by ROM	0.9134	0.8114	0.9009	0.9690	0.9690
Relative error		0.04%	0.27%	0.12%	0.12%
Parameter in constrain					
T_4 (Peak temperature, K) in optimization using ANN		2400	2500	2600	2620.2
T_4 (Peak temperature, K) run by ROM	2663.1	2399.8	2501	2605.3	2627.2
Relative error		0.01%	0.04%	0.20%	0.27%

3.5 Multi-objective optimization

Another key performance indicator of an IGCC gasifier is the composition of the syngas it produces. Specifically, specific syngas components such as H_2 require lower operating conditions than others, and it is thus beneficial to maximize the molar fraction of hydrogen in the final syngas composition so as to improve its efficiency. In an ideal gasifier system, it is desirable to maximize both the carbon conversion and the production of H_2. However, these two objectives have been observed to be in conflict with each other, as the input conditions required to maximize carbon conversion negatively impact the hydrogen production, and vice versa.[13] Motivated by this, a

second optimization study was performed with the aim to analyze the relationship and determine the optimal trade-off conditions between these two conflicting objectives. This multi-objective optimization study was performed with respect to each of the input parameters $\boldsymbol{P}$ mentioned in Section 3.2.1 according to the following optimization formulation:

$$\max_{\boldsymbol{P}}[(1-w)\,T_1(\boldsymbol{P}) + wT_3(\boldsymbol{P})] \tag{5}$$

Subject to:
$ANN\ model$

$T_4\ (\boldsymbol{P}) \leq T_{4,max}$

$\boldsymbol{P}_{min} \leq\ \boldsymbol{P} \leq\ \boldsymbol{P}_{max}$

where the parameter w is a weight which denotes the significance of each of the individual objective functions, i.e., carbon conversion (T_1) and hydrogen molar fraction in outlet (T_3). In the above optimization formulation, the maximum allowed peak temperature was fixed at $T_{4,max} =$ 2,600 K based on the optimization results obtained for the first case study discussed above. Furthermore, the upper and lower bounds $\boldsymbol{P}_{max}$ and $\boldsymbol{P}_{min}$ are defined by the values listed in Table 3. For this multi-objective optimization study, the weight parameter w was changed from 0 to 1 by increment of 0.1. The results of the multi-objective optimization obtained using the ANN model were validated by running the ROM as shown in Table 9. Note that the errors between the two modeling methods remained below 2.2%, showcasing that the ANN is capable of predicting the gasifier behaviour with sufficient accuracy compared to the ROM. Figure 10 provides a graphical illustration of the pareto front for the feasible search space accessible to the gasifier model that is formed based on the solutions to problem (5).

Table 9. Multi-objective optimization results

parameter name	w = 0	w = 0.1	w = 0.2	w = 0.3	w = 0.4	w = 0.5	w = 0.6	w = 0.7	w = 0.8	w = 0.9	w = 1	1-norm
P_1 (Fuel Flow Rate, kg/h)	40	40	40	40	40	40	40	40	40	40	52.3	40
P_2 (O_2 Flow Rate, kg/h)	37.2	37.2	37.2	37.2	37.2	37.2	37.2	37.2	37.2	28.4	28.4	28.4
P_3 (N_2 Flow Rate, kg/h)	11	11	11	11	11	11	11	11	11	11	11	11
P_4 (Steam Flow Rate, kg/h)	19.2112	19.5424	19.9225	20.366	20.8952	21.5464	21.8	21.8	21.8	18.1061	14.5294	18.0935
P_5 (Fuel Temperature, K)	330	330	330	330	330	330	330	330	330	330	330	330
P_6 (Mass Fraction Ash)	0.0506	0.0506	0.0506	0.0506	0.0506	0.0506	0.0506	0.0506	0.0506	0.0506	0.0506	0.0506
P_7 (Mass Fraction Volatiles)	0.1397	0.1397	0.1397	0.1397	0.1397	0.1397	0.1397	0.1397	0.1397	0.1397	0.1397	0.1397
P_8 (Mass Fraction Moisture)	0.0055	0.0055	0.0055	0.0055	0.0055	0.0045	0.0055	0.0055	0.0055	0.0045	0.0045	0.0045
Optimized parameter												
T_1 (Conversion) results using ANN	0.9702	0.9702	0.9701	0.9701	0.9699	0.9697	0.9696	0.9696	0.9696	0.7494	0.5471	0.7494
T_1 (Conversion) results using ROM	0.9690	0.9690	0.9689	0.9688	0.9687	0.9684	0.9683	0.9683	0.9683	0.7492	0.5476	0.7492
Relative error	0.12%	0.12%	0.12%	0.13%	0.12%	0.13%	0.13%	0.13%	0.13%	0.03%	0.09%	0.03%
T_3 (H_2 molar fraction) results using ANN	0.2400	0.2401	0.2404	0.2406	0.2408	0.2411	0.2412	0.2412	0.2412	0.265	0.2836	0.265
T_3 (H_2 molar fraction) results using ROM	0.2354	0.2356	0.2357	0.2358	0.2359	0.2360	0.2360	0.2360	0.2360	0.2638	0.2843	0.2638
Relative error	1.95%	1.91%	1.99%	2.04%	2.08%	2.16%	2.20%	2.20%	2.20%	0.45%	0.25%	0.45%

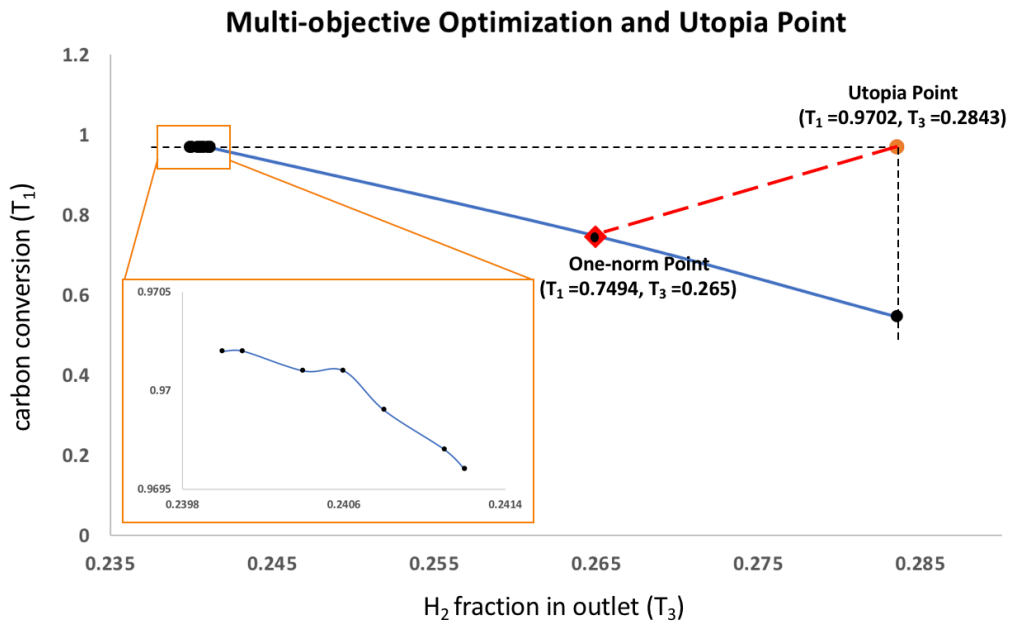

Figure 10. Multi-objective optimization: pareto front, utopia point and 1-norm point

As indicated in this figure and in Table 9, when w increases, the mole fraction of H_2 in the outlet syngas increases whereas the carbon conversion decreases, as was expected. Note that since the carbon conversion values (T_1) are much larger than the hydrogen molar fraction values (T_3), there is a slowly-decreasing trend of the results of carbon conversion between w = 0 and w = 0.8. When w reaches 0.9, the value of $wT_3(\boldsymbol{P})$ is similar to $(1-w)T_1(\boldsymbol{P})$, and consequently the optimized H_2 fraction begins to rise significantly whereas the carbon conversion starts to decrease drastically corresponding to the notable decrease in the oxygen-to-fuel ratio at w = 0.9.

In order to determine the ideal trade-off point between the carbon conversion and the hydrogen production, the ANN gasifier model was implemented into a 1-norm bi-objective optimization scheme. This optimization approach seeks to minimize the 1-norm distance between the feasible search space, as defined by the pareto front, and the utopia point (i.e., the infeasible point that optimally satisfies both objectives simultaneously),[74] in order to determine which set of feasible

conditions yield results that are closest to the utopia point (measured in terms of a 1-norm distance). The 1-norm minimization problem can be formulated as follows:

$$\min_{\mathbf{P}} \left[\frac{T_{1,max} - T_1(\boldsymbol{P})}{T_{1,max} - T_{1,min}} + \frac{T_{3,max} - T_3(\boldsymbol{P})}{T_{3,max} - T_{3,min}} \right] \quad (6)$$

Subject to:
$ANN\ model$

$T_4\ (\boldsymbol{P}) \leq T_{4,max}$

$\boldsymbol{P}_{min} \leq\ \boldsymbol{P} \leq \boldsymbol{P}_{max}$

where $T_{1,max}$ and $T_{3,max}$ denote the maximum conversion and H_2 molar fractions obtainable within the optimization constraints of problem (5) and define the utopia point, ($T_{1,max}$, $T_{3,max}$). Note that the maximum conversion ($T_{1,max}$) and minimum H_2 molar fraction ($T_{3,min}$) values are obtained by solving a single-objective optimization study that maximizes the carbon conversion, i.e., when $w = 0$ in problem (5); similarly, the minimum conversion ($T_{1,min}$) and maximum H_2 fraction ($T_{3,max}$) values are obtained by solving the optimization study that maximizes the hydrogen production, i.e., when $w = 1$. In addition, the constraint parameters $\boldsymbol{P}_{min}$, $\boldsymbol{P}_{max}$, and $T_{4,max}$ were fixed to the same values used in problem (2). The results of this optimization study are listed in Table 9 (1-norm); in addition, the utopia point and the optimal trade-off point are denoted in Figure 10. Under these optimal conditions, the carbon conversion $T_1 = 0.7494$ is at 52.2% of the utopia point conversion, whereas the molar fraction of H_2 in the outlet syngas $T_3 = 0.265$ is at 42.7% of the syngas hydrogen fraction at the utopia point, as shown in the Figure 10. These results reveal that it is not possible to significantly improve the hydrogen production within the gasifier without noticeably reducing the carbon conversion. Note that the ANN model required about 0.1617 s of CPU time to determine the optimized results for the multi-objective optimization described above. However, it is challenging to conduct the same optimization study using the ROM model due to the computation costs; hence, this demonstrates that the ANN is significantly more

computationally efficient compared to the ROM, while achieving sufficiently similar results. Hence, the optimization using ANN shows that it is particularly efficient and accurate to perform optimization studies on the pilot-scale gasification unit.

3.6 Summary

The aim of this chapter was to present an ANN model composed of eight sub-networks that can predict the stationary operation of an IGCC gasification system. The number of neurons in the hidden layer of ANN model were determined via optimization for each sub-network. In addition, Levenberg-Marquardt was selected as the back-propagation algorithm for training. This method provided the fastest and most reliable network training when compared to eight different training algorithms. Subsequently, the ANN model was successfully validated and was able to accurately predict the gasifier outputs at significantly lower computational costs compared to the ROM model. The validated ANN model was used to perform two different optimization studies. Those studies showed that increasing the peak temperature constraint in the reactor would cause a higher maximum carbon conversion. Also, the results from a multi-objective optimization formulation showed that it is very unlikely to improve H_2 production in the gasifier without reducing the carbon conversion. The results presented in this chapter assumed that the gasifier operates at steady-state; nevertheless, the operation of a gasification units is often subject to transient changes that occur in the IGCC plant; hence the need to develop an inexpensive time-dependent model that considers the transient operation of these units.

Chapter 4
Modelling and Optimization of a Pilot-scale Entrained-Flow Gasifier using Reccurent Neural Networks

This chapter presents the construction and validation of a recurrent neural network (RNN) that can efficiently predict the dynamic performance of a pilot-scale gasifier unit. The RNN model consists of a set of sub-networks that predict the transient behavior of the each of the key process outputs as a function of the input parameters of the pilot-scale gasifier. The performance of the RNN was compared to a dynamic ROM model, which was validated using experimental data and computational fluid dynamics. The RNN model was embedded within an optimization formulation to investigate the optimal operation of a gasifier under key operational constraints. The results from these optimization studies illustrate the benefits of the RNN, which were able to identify optimal time-dependent profiles in key input variables that improve the efficiency and availability of the gasifier under load-following and co-firing. Most of the results of this chapter has been submitted for publication to Fuel.[75]

4.1 Introduction of dynamic ROM

The dynamic behavior of an IGCC gasifier can become computationally expensive to simulate using CFD;[32] hence, one-dimensional reduced order models (ROMs) are most commonly used to simulate the transient operation of these units. ROMs have been developed to provide detailed gasifier performance data as a function of key inputs to this system, such as the feed composition and the inlet reactor flow patterns. The present work considers a dynamic ROM previously presented by Sahraei et al. that considered the gasifier as a reactor network consisting of two continuous stirred-tank reactors (CSTRs) and three plug-flow reactor (PFRs), which aim to capture the gasifier's laminar and mixing flow structures.[24,12] That ROM was used to simulate a

pilot entrained-flow IGCC gasifier owned by CanmetENERGY, Natural Resources Canada; this system is presented in Figure 2.[24] The dynamic ROM reactor network decomposes the pilot entrained flow gasifier into three types of zones referred to as the jet expansion zone (JEZ), the external recirculation zone (ERZ), and the down-stream zone (DSZ), as illustrated in Figure 5. In this model, the JEZs and DSZ are modeled using PFRs, whereas CSTRs are used to model the ERZs. More details about the description of the gasifier, its configuration parameters and the reactor network flow pattern can be found elsewhere.[24,12] In order to estimate the velocity profiles, species compositions and temperature profiles of the multi-phase flow inside the pilot-scale gasifier, the ROM solves the mass, energy, and momentum balance equations for the gas, liquid and solid phases within each zone inside the gasifier. A full list of these equations for the present dynamic model are listed in Table 10. The key input parameters of the dynamic ROM are the inlet flow rate of the fuel, steam, oxygen, nitrogen, and limestone (CaO), as well as the percent composition of ash, volatiles, and moisture within the fuel. A more detailed description of the inlet flow rate for different feedstocks and the reactor network flow patterns is presented elsewhere.[12]

Table 10. Mathematical model of the multi-phase flow in the dynamic ROM[24]

Gas phase	
Velocity	$\frac{\partial(\mathrm{A_{cs}}\varepsilon_g\rho_g u_g)}{\partial t} = -\frac{\partial}{\partial z}(\mathrm{A_{cs}}\varepsilon_p\rho_p u_g^2) + A_{cs}(-\frac{dP}{dz} + \varepsilon_g\rho_g g - F'_{g\rightarrow wall} - F'_{g\rightarrow p})$
Molar composition	$\frac{\partial}{\partial t}(\mathrm{A_{cs}}\varepsilon_g C_{total} x_i) = \frac{\partial}{\partial z}\left(\mathrm{A_{cs}} D_{g,eff}\frac{\partial(\varepsilon_g C_{total} x_i)}{\partial z}\right) - \frac{\partial(\mathrm{A_{cs}}\varepsilon_g u_g C_{total} x_i)}{\partial z} + A_{cs}(R_{hom} + R_{het})$
Temperature	$\frac{\partial\left(\mathrm{A_{cs}}\varepsilon_g C_{total} c_{p_g} T_g\right)}{\partial t} = \frac{\partial}{\partial z}\left(\mathrm{A_{cs}} k_{g,eff}\frac{\partial T_g}{\partial z}\right) - \frac{\partial\left(\mathrm{A_{cs}}\varepsilon_g u_g C_{total} c_{p_g} T_g\right)}{\partial z} + A_{cs}(R_{hom} H_R) + Q'_{convg\rightarrow p} - Q'_{convg\rightarrow p}$
Solid phase	
Velocity	$\frac{\partial}{\partial t}(\mathrm{A_{cs}}\varepsilon_p\rho_p u_p) = -\frac{\partial}{\partial z}(\mathrm{A_{cs}}\varepsilon_p\rho_p u_p^2) + \mathrm{A_{cs}}(\varepsilon_p\rho_p g + F'_{g\rightarrow p})$
Mass flow rate	$\frac{\partial(M_{solid}/u_p)}{\partial t} = -\frac{\partial(M_{solid})}{\partial z} + A_{cs}(R_{het}) - m'_{slagging}$
Temperature	$\frac{\partial}{\partial t}\left(A_{cs}\varepsilon_p\rho_{solid} c_{p_p} T_p\right) = -\frac{\partial}{\partial z}\left(A_{cs}\varepsilon_p u_p\rho_p c_{p_p} T_p\right) + A_{cs}(R_{het} H_R) - Q'_{conv\rightarrow g} - m'_{slagging} h_p$
Particle density	$\frac{\partial(A_{cs} N_p)}{\partial t} = \frac{\partial(A_{cs} N_p u_p)}{\partial z} + \frac{m'_{slagging}}{m_p}$
Liquid phase	
Slag mass	$2\pi r_{gasifier}\rho_{slag}\frac{\partial(\delta_{slag})}{\partial t} = -\frac{\partial m_{slag}}{\partial z} + m'_{slagging}$
Particle density	$2\pi r_{gasifier}\rho_{slag} C_{P_{slag}}\frac{\partial(T_{slag}\delta_{slag})}{\partial t} = 2\pi r_{gasifier} k_{slag}\frac{\partial}{\partial z}\left(\delta_{slag}\frac{\partial T_{slag}}{\partial z}\right) - \frac{\partial}{\partial z}\left(m_{slag} T_{slag} C_{P_{slag}}\right) + Q'_{convg\rightarrow slag} + Q'_{convslag\rightarrow surronding} + m'_{slagging} H_p$

Note that in the dynamic gasifier system modeled using the ROM, the fuel type could change over the course of the operation and thus the composition of the fuel can vary significantly over time. Also, the variability in the fuel's ash composition can significantly affect the gasifier's availability,

since the ash is formed and melted inside the gasifier at high operating temperatures. Most of the ash deposits on the gasifier's wall and leaves the gasifier as a form of slag that may cause clogging within the unit.[24,76] Consequently, limestone is added to the gasification unit as a fluxant to reduce the viscosity of the slag and to avoid blockage within the entrained flow gasifier. Therefore, a minimum CaO mass of 21% with respect to the fuel fed into the gasifier is required to maintain a lower slag viscosity and prevent slag blockage.[24] The present work considers two types of fuel to be fed into the gasifier unit: Alberta petroleum coke and Genesee coal. Molar compositions for each type of fuel are shown in Table 11.

Table 11. Fuel composition

	Alberta petroleum coke (%)	Genesee coal (%)
ash	0.046	0.247
volatiles	0.127	0.269
moisture	0.005	0.061
carbon	0.822	0.423

The performance of a gasifier can be described by the conversion of its reactants, the concentration of its desired products at the gasifier's outlet and the temperature distribution throughout the unit.[25] In addition, the viscosity and thickness of the deposited ash slag are two additional essential system parameters that can be used to characterize the dynamic performance of the gasification unit. At the reactor outlet, critical system parameters such as the carbon conversion and the molar fraction of key gasifier syngas products (i.e., CO and H_2) provide important measurements that indicate the performance of the gasification unit and its ability to convert the solid input fuel into a more-desirable syngas. Another significant observable of the gasification system is the internal temperature distribution within the reactor, i.e., the reactor's

peak temperature and the temperature measured with the thermocouples located inside the gasifier. The peak temperature of gasifier is of particular importance as it is critically necessary to guarantee that the reactor temperature will at no point increase beyond the maximum temperature that the gasifier's refractory wall layer can bear.[77] As shown in Figure 2, the temperature is monitored at key locations along the unit corresponding to the locations of thermocouples within an actual gasifier unit. Furthermore, the gasifier performance within a dynamic IGCC plant is significantly affected by the viscosity and thickness of the slag formed by the deposited molten ash, since the slag collected along the wall of gasifier may lead to blockage near the outlet of the unit if the viscosity and thickness of slag are high.[76] These output parameters are the dominant factors playing an important role for the ash particles to stick inside the gasification unit, and thus they have a significant influence on the gasifier's availability.

In dynamic gasification systems, the inlet flowrates and fuel composition can change over time depending on the nature of the IGCC power plant, the requested power demands and potential disturbances that may affect the unit during operation.[24] There are two primary scenarios typically considered in IGCC power production: load-following and co-firing. In the first, the power generation can be adjusted during operation by manipulating the fuel loading according to the electricity demands as well as the power supply from alternate energy sources.[78] For the co-firing scenario, power plants often burn different type of fuels (i.e., coals) to maintain continuous operation and improve the availability of the fuel and the efficiency of the unit. In this work, the dynamic the performance of the pilot entrained-flow gasifier is analyzed under the conditions that are likely to occur during operation, i.e., co-firing and load-following.

Table 12 presents the operational conditions considered in this study for the gasification unit. As shown in this table, the gasifier can operate between a near full capacity and a minimum partial load capacity, which is restricted to 70% of the plant's full capacity, due to the high operating cost of IGCC power plant. The changes in the operating conditions of this pilot entrained flow gasifier

are implemented via a reduction of the load from the peak load condition to a minimal partial load with a ramp rate of 5% per min and increasing it back to the peak value at a ramp rate of 3.3% per min. During these changes in fuel load, the ratios of oxygen/fuel and steam/fuel are maintained to avoid the temperature exceeding the thermal constraint of the refractory wall. Note that the ramping rate in the feed flowrate of the fuel is restricted to a maximum ramp of 5% per min as the changes in the operating conditions may limit the life span of the refractory of the gasifier. Also, the ramping up process is typically slower than ramping down due to the nature of gasification process and gas turbine flexibility.[78] Moreover, limestone/ash weight ratio remains fixed at 21% to keep the viscosity of the slag less than 25 Pa s and thus avoid clogging near the outlet of the gasifier reactor. In most of the coal gasification units, the viscosity of coal exponentially decreases with an increase in temperature and the slag with viscosity below 25 Pa s flows down the gasifier walls and is discharged through the tapping device.[79] To perform co-firing while at full fuel-load capacity, the feedstock was linearly changed (3.33% per min) from Alberta petroleum coke feed to a 60:40 blended feed of petroleum coke and Genesee coal. Note that the oxygen/fuel and steam/fuel ratios were also maintained constant during co-firing to avoid any damage to the refractory brick layer due to changes in temperature. Both load-following and co-firing have been used in the present analysis for the identification of the RNN model for this unit, which is described next.

Table 12. Operating condition of the pilot-scale gasifier in IGCC

	Full capacity	Minimum partial load (70% capacity)
Fuel (kg/h)	41.2	28.84
Oxygen (kg/h)	37.2	26.04
Steam (kg/h)	10.7	7.49

4.2 Development of recurrent neural network model

Recurrent neural networks (RNN) are a class of artificial neural networks that feed the outputs of the system neurons back to themselves, to other adjacent neurons, or to neurons within preceding network layers. The most relevant property of RNN is that they manifest highly nonlinear transient behavior and return the outputs as feedbacks to the input layer in a time sequence; this makes RNNs a helpful tool to model the nonlinear relation between the input and output parameters of complex dynamic systems such as a gasification unit.[80] Although traditional black box models are available to perform identification for dynamic systems, e.g., ARX or ARMAX, they are still linear models. In the case of an RNN model, their model structure contains nonlinear activation functions inside each neuron of the hidden layers, which makes them efficient and sufficient to capture the transient performance of highly nonlinear systems. Consequently, this work considers a recurrent neural network architecture to predict the key outputs of the gasification unit (i.e., the carbon conversion, syngas composition, temperature profile and ash slag properties) for a given set of inlet gas flowrates and fuel compositions. As shown in Figure 11, the gasifier's RNN model was developed as a network of sub-RNNs such that each sub-RNN predicts the performance of each output parameter individually as a function of the input parameters at the current time as well as the output parameter values at previous time steps.

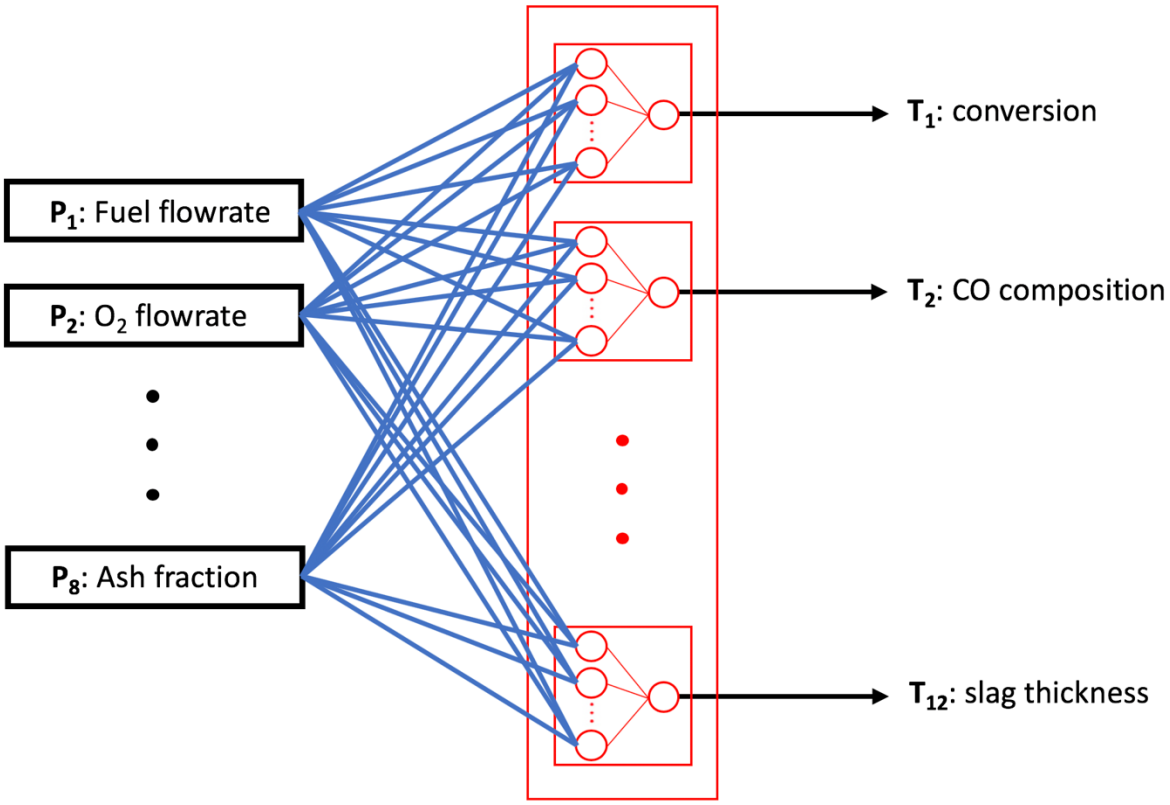

Figure 11. Brief structure of recurrent neural network model for all key outputs

All input parameters and output parameters used for the identification of the RNNs model are listed in Table 13. As depicted in Figure 12, each sub-RNN consists of a shallow, two-layer structure comprised of a hidden layer with a tan-sigmoid transfer function and an output layer with a linear transfer function. In the output layer, the output is connected back to the input layer as the feedback. The complete RNN gasifier model was trained using data derived from the dynamic ROM. The following sections describe the design, training and optimization of the RNN model considered in this study.

Table 13. Input and output parameters for the gasifier

Input parameters (***P'***)	Nominal conditions ($\boldsymbol{P_{nom}}$)	Initial conditions ($\boldsymbol{P^{t0}}$)	Lower bound ($\boldsymbol{P_{min}}$)	Upper bound ($\boldsymbol{P_{max}}$)
P'_1: Fuel flowrate (kg/h)	41.2	41.2	28.84	43.26
P'_2: O2 flowrate (kg/h)	37.2	37.2	26.04	39.06
P'_3: N2 flowrate (kg/h)	12.1	12.1	11.0	12.1
P'_4: Steam flowrate (kg/h)	10.7	10.7	7.49	11.235
P'_5: Limestone (CaO) flowrate (kg/h)	0.416	0.416	0.34	4.56
P'_6: Mass fraction of ash in fuel	0.046	0.046	0.046	0.1026
P'_7: Mass fraction of volatiles in fuel	0.127	0.127	0.127	0.1397
P'_8: Mass fraction of moisture in fuel	0.005	0.005	0.005	0.0201

Output parameters (***T***)	Output values at nominal condition
T_1: Conversion	0.9134
T_2: Outlet CO composition	0.5135
T_3: Outlet H2 composition	0.2176
T_4: Peak temperature (K)	2663.1
T_5: Temperature: Thermocouple 1 (K)	1911.4
T_6: Temperature: Thermocouple 2 (K)	1786.4
T_7: Temperature: Thermocouple 3 (K)	1672.6
T_8: Temperature: Thermocouple 4 (K)	1609.0
T_9: Maximum refractory temperature (K)	1911.4
T_{10}: Refractory temperature at outlet (K)	1609.0
T_{11}: Slag viscosity (Pa s)	12.3
T_{12}: Slag thickness (mm)	1.055

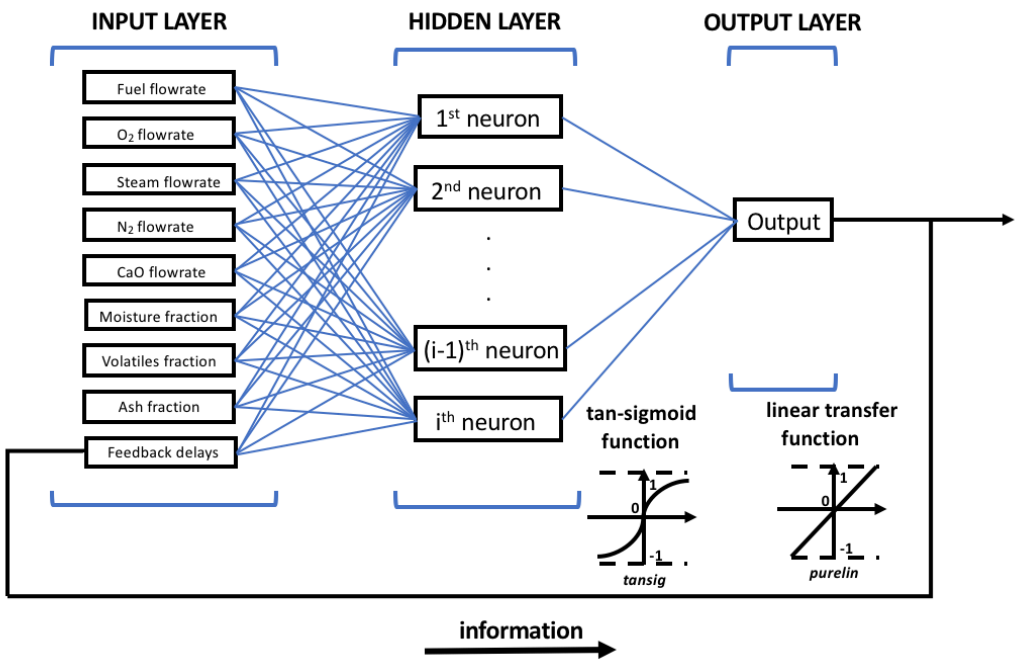

Figure 12. Detailed structure of a sub-network for one key output

4.2.1 Overview of recurrent neural networks

In a recurrent neural network architecture, the dynamics of a system can be estimated by treating the predicted model outputs and the process inputs at previous sampling instances as input data for the current network predictions.[81] That is, the inputs to the network for a dynamic process at a given sampling point consist of the current process inputs and predicted outputs from previous sampling points. As shown in Figure 13, an RNN can operate under two modes: i) open-loop mode, which is used during training of the network and uses the outputs from the process as inputs to the network at each time interval; and ii) closed-loop mode, which is implemented during the testing and validation stages and consists of using the output predictions coming from the RNN model at the current time interval as inputs to the RNN to predict the output for the next time interval. The latter represents the actual scheme of operation of the RNN model considered in this work.

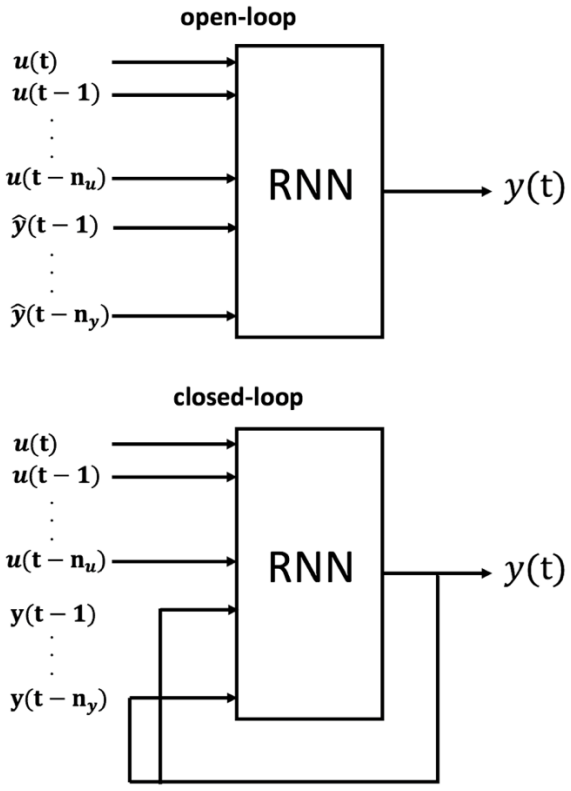

Figure 13. Two important modes of recurrent neural network

The nonlinear autoregressive network with exogenous inputs (NARX) model is a recurrent dynamic network with feedback connections enclosing several layers of the network which is commonly used in time-series modeling; thus, it is particularly suitable for nonlinear dynamic systems identification. In this auto-regressive scheme, the system output at a time step $\boldsymbol{t}$ is modelled as a nonlinear mapping of the previous values of the system inputs and outputs, in addition to the current input parameter values, i.e.,

$$\boldsymbol{y}(t) = \boldsymbol{g}\left(\boldsymbol{u}(t), \boldsymbol{u}(t-1), \dots, \boldsymbol{u}(t-n_u), \boldsymbol{y}(t-1), \boldsymbol{y}(t-2), \dots, \boldsymbol{y}\left(t-n_y\right)\right) \quad (7)$$

where the next value of the dependent output signal $\boldsymbol{y}(\boldsymbol{t})$ is regressed on previous values of the output signals $\boldsymbol{y}(\boldsymbol{t}-\boldsymbol{1}), \dots, \boldsymbol{y}\left(\boldsymbol{t}-\boldsymbol{n_y}\right)$ whereas $\boldsymbol{u}(\boldsymbol{t}), \boldsymbol{u}(\boldsymbol{t}-\boldsymbol{1}), \dots, \boldsymbol{u}(\boldsymbol{t}-\boldsymbol{n_u})$. $\boldsymbol{u}(\boldsymbol{t})$ represent the

values of the input signals at the current time step; $\boldsymbol{n_u}$ and $\boldsymbol{n_y}$ are discrete time-indexes that denote the finite time delay of the input and output signals, respectively. $\boldsymbol{g}(\cdot)$ represents the predictor function applied to the system.

In this work, we employed an RNN model based on the NARX architecture shown in (7), as depicted in Figure 14. The terms $\mathbf{R}$, $\mathbf{S^1}$and $\mathbf{S^2}$ in Figure 14 represent the dimensions of the inputs, weights and bias matrices in the hidden and output layers, respectively. The complete RNN model can be described as follows:

$$y(t) = f_2(\boldsymbol{W}_2(f_1(\boldsymbol{W}_1\emptyset(t) + \boldsymbol{b}_1)) + \boldsymbol{b}_2 \tag{8}$$

where $\boldsymbol{f_1}$ represents the nonlinear activation sigmoid function in the hidden layer, $\boldsymbol{f_2}$ represents the linear function in the output layer; similarly, $\boldsymbol{W_1}$ and $\boldsymbol{W_2}$ represent the matrices of network weights connecting the input layer to the hidden layer and the hidden layer to the output layer, respectively. Note that the weighting matrices $\boldsymbol{W_1}$ and $\boldsymbol{W_2}$ have dimensions $\mathbf{S^1}$x$\mathbf{R}$ and $\mathbf{S^2}$x$\mathbf{S^1}$, respectively. In addition, $\boldsymbol{b_1}$ and $\boldsymbol{b_2}$ represent the bias terms for the functions $\boldsymbol{f_1}$ and $\boldsymbol{f_2}$, respectively. The function $\emptyset(\boldsymbol{t})$ is represented as follows:

$$\emptyset(t) = \left[\boldsymbol{u}(t), \boldsymbol{u}(t-1), \dots, \boldsymbol{u}(t-n_u), \boldsymbol{y}(t-1), \boldsymbol{y}(t-2), \dots, \boldsymbol{y}\left(t-n_y\right)\right] \tag{9}$$

The RNN training is the process of finding the weights and the biases of the network, i.e., $\boldsymbol{W_1}$, $\boldsymbol{W_2}$, $\boldsymbol{b_1}$ and $\boldsymbol{b_2}$, such that the underlying training model captures the nonlinear dynamic behavior of the actual system. That is, the objective of the training process is to minimize a loss function often represented as the sum of the mean squared errors (MSE), i.e.,

$$\text{MSE} = \frac{1}{N}\sum_{t=1}^{N}(\boldsymbol{y}(t) - \widehat{\boldsymbol{y}}(t))^2 \tag{10}$$

where $\widehat{\boldsymbol{y}}$ and $\boldsymbol{y}$ represent the target data and the output prediction of the RNN model at time t. In this study, the loss function is minimized using the Levenberg-Marquardt algorithm via feeding

the data set (i.e., the training data set). In order to avoid overfitting in the RNN model, it is necessary to analyze the RNN performance during training in order to prevent the network from simply memorizing the training data. An early stopping method was employed in this work for the RNN training algorithm, which sub-divided the input-output dataset into three parts: the training set, the validation set, and the testing set. The training set is used to optimize the weights of each neuron so as to minimize the errors between $\mathbf{y}(\mathbf{t})$ and $\hat{\boldsymbol{y}}(\mathbf{t})$ as shown in equation (10). After each epoch of training, the network is fed with the input data from the validation set and used to predict the network output under these conditions. This process continues until the validation error is either sufficiently small or it does not significantly change after a certain number of successive epochs. Once the training has been completed, the testing dataset is used to validate the performance of the RNN model. If the testing error obtained from this process is insufficiently small, then the input-output data is redistributed between three datasets and the network is re-trained until the errors fall below a user-defined criterion.

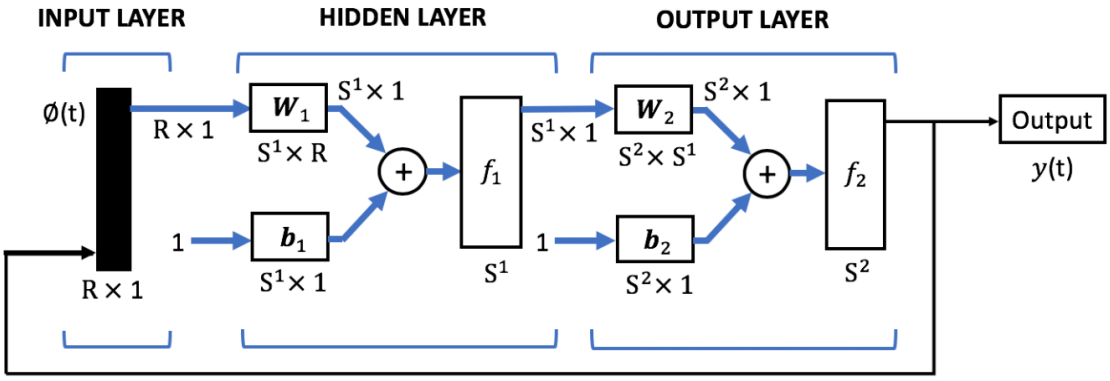

Figure 14. RNN model based on the NARX architecture

4.2.2 Input and output training data

Table 13 shows the key input parameters (***P'***) that affect the gasifier's transient performance. The flowrate of the fuel (P'_1), oxygen (P'_2), nitrogen (P'_3) and steam (P'_4) have been restricted to the upper and lower bounds shown in this table. These bounds match with the operating conditions at which the dynamic ROM was developed, as well as the experimental tests on the pilot entrained-flow gasifier used to validate the ROM. Note that the lower and upper bounds of fuel composition parameters (i.e., P'_6, P'_7, & P'_8 in Table 13) were defined based on the two types of fuels used in this study, i.e., Alberta petroleum coke and Genesee coal. Table 13 also lists the output parameters (***T***) as well as their corresponding minimum and maximum values over which the RNN model was trained. More information about each of these input and output parameters can be found in Section 4.1. Similar to the input parameters ***P'***, the range of values for each ***T*** was determined based on the range of allowable values used in the development of the dynamic ROM and the experimental tests on the pilot-scale gasifier that were used to validate the ROM.

As described in Section 4.1, the load-following and co-firing scenarios were used in the present study to analyze the gasifier's dynamic performance within the range of operating conditions considered for that unit. An overview of the identification test used to identify the RNN is illustrated in Figure 15. For this study, cycles consisting of a combination of co-firing and load-following were run continuously until a sufficiently large number of cycles that are acceptable for systems identification was reached. Each cycle includes two regions for load-following. On each of these regions, the fuel load is changed using ramps until it reaches the targeted load set-point. After each ramp test in the load-following, two cycles of co-firing are performed. During co-firing, the composition of the fuel is changed in a ramp fashion until it reaches a specified target (i.e., a ratio between the types of fuels considered in this work). As shown in Figure 15, the fuel load is initially set at the full capacity using petroleum coke as the fuel (i.e., r1 in Figure 15). Then, load-following is performed (r2 in Figure 15); in this region, the plant's fuel load of pet-coke is gradually modified

such that it decreases to a pre-set partial load at a ramp rate of 5% per minute. Co-firing is performed next (i.e., r3 in Figure 15), the fuel load is maintained at the pre-set partial load condition (i.e., constant fuel loading), the feedstock is linearly changed in a ramp fashion from a pure petroleum coke feed to a blended feed of petroleum coke and coal, as shown at the bottom of Figure 15. In region 4 (r4 in Figure 15), the plant's fuel load of mixture feed is gradually increase back to a pre-set high fuel load in a ramp fashion at a rate of 3.3% per minute. When the feed load reaches region 5 (r5 in Figure 15), the fuel load is kept at the pre-set partial load (constant loading) condition whereas the feedstock is ramped back from the blended feed of petroleum coke and coal to the pure petroleum coke (i.e., co-firing). This cycle is repeated multiple times until sufficiently enough data has been gathered from the dynamic ROM to perform the identification of the RNN model. Note that the fuel composition is maintained at a particular value during load-following cycles, whereas the fuel loading is maintained during the co-firing cycles, as shown in Figure 15. For each cycle, the partial fuel load is set to a random uniformly-selected value between 70% and 100% of the peak fuel flow rate under load-following conditions. Likewise, the ratio of the blended feed under co-firing conditions is randomly selected from a uniform distribution between a 100:0 ratio (i.e., pure petroleum coke) and a 60:40 ratio of petroleum coke to coal. As shown in Figure 15, the oxygen to fuel and steam to fuel ratios remained constant to prevent the peak system temperature from exceeding the thermal constraint of the gasifier refractory wall layer. Moreover, during each cycle, the CaO/ash weight ratio is maintained at a randomly-generated value chosen from a uniform distribution between 15% and 25%. This range of values was selected since it reflects the range of values at which dynamic ROM was developed (i.e., the nominal value of CaO/ash is 21%).

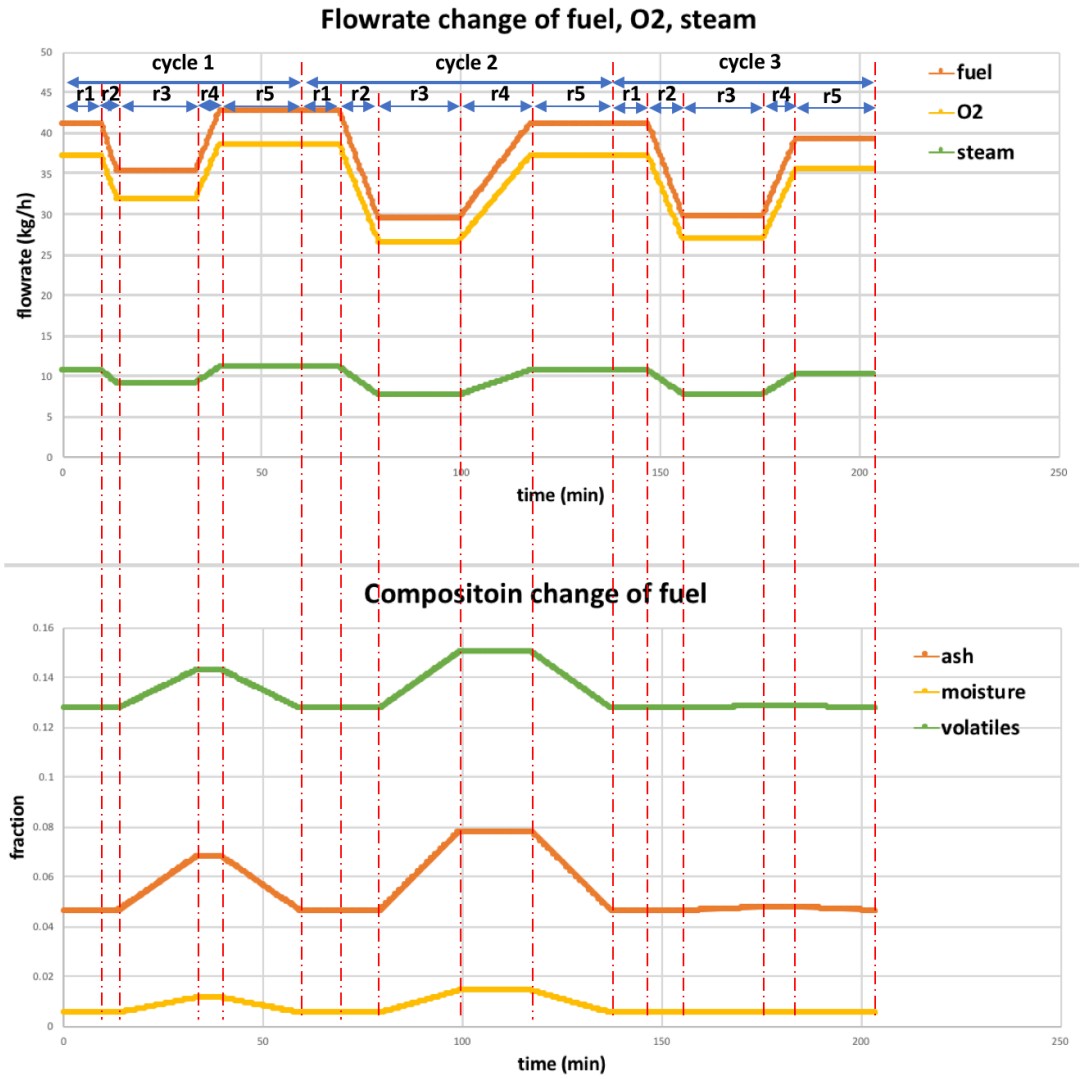

Figure 15. An overview of the identification test

A set of 40,000 data points involving 50 cycles were collected from the ROM to train the RNN. Each data point contains information of the input variables (**P'**) and the corresponding outputs (**T**) at each time interval, which was set 10 seconds. The purpose of generating such a large dataset was to ensure that the RNN model would have sufficiently enough information to capture the transient characteristics of the gasification unit that are likely to occur during operation. The data was divided into three datasets: 35 cycles for training dataset, 10 cycles for validation dataset, 5 cycles for testing.

4.2.3 Recurrent neural network structure

The aim of this section is to perform optimization on the number of hidden layer neurons for each of the 12 sub-RNNs developed in this work to predict the dynamics between each of the inputs and outputs considered in the gasifier unit. Each sub-network was developed using the two-layer architecture described previously. As indicated above, the Levenberg-Marquardt algorithm was employed to train the RNN. To optimize the structure of RNNs model, each sub-network was initialized with a hidden layer containing only one single neuron, and the sub-networks were trained to predict each of the outputs listed in Table 13 as a function of all the input variables. Consequently, the number of neurons in each hidden layer was incremented by one for each identification run and the networks were re-trained using the same identification data. The mean squared errors (MSE) were calculated as shown in equation (10) for the validation and testing tests using the data for each network. This process was repeated until overfitting was detected, i.e., when the sub-network's validation error decreased but its testing error increased; at this point, the optimization process was terminated. This procedure was repeated for each sub-network considered in the RNN. Identification of the RNN model was performed using the Neural Network Toolbox available in Matlab 2017.

The performance of the structures considered for each of the RNN developed in this work are shown in Table 14. As shown in this table, the mean percentage error obtained for each output (T) during the validation test is less than 5%; also, the maximum percentage errors between the predictions obtained by the RNN and the target output generated by ROM for the test and validation sets in the training process are sufficiently low, i.e., below 8.5%. Note that the maximum percentage error between the test and validation sets are similar to each other for each output parameter, which is an indication that there is no overfitting on each sub-RNN model.

Table 14. Results from the RNN identification

Output parameters	No. of neurons	Mean percentage error		Maximum percentage error	
		test	validation	test	validation
Conversion (T_1)	5	0.98%	0.99%	1.53%	1.51%
CO composition (T_2)	4	0.62%	0.72%	1.78%	1.71%
H_2 composition (T_3)	3	0.68%	0.70%	0.86%	0.82%
Peak temperature (T_4)	5	0.30%	0.48%	1.33%	1.02%
Thermocouple 1 (T_5)	6	0.60%	0.61%	4.08%	3.65%
Thermocouple 2 (T_6)	6	0.44%	0.50%	2.92%	2.58%
Thermocouple 3 (T_7)	6	0.58%	0.61%	1.62%	1.22%
Thermocouple 4 (T_8)	6	0.48%	0.65%	1.66%	1.21%
Maximum refractory temperature (T_9)	6	0.51%	0.87%	4.03%	3.57%
Refractory temperature at outlet (T_{10})	6	0.68%	0.71%	1.61%	1.23%
Slag viscosity (T_{11})	5	2.54%	2.26%	5.63%	5.54%
Slag thickness (T_{12})	8	2.84%	4.41%	7.97%	8.21%

4.2.4 RNN Model Performance

The aim of this section is to compare the performance of the RNN described in Section 4.2.3 to fresh new data that was not used during the identification of the RNN model. Hence, the RNN's performance was compared with the predictions obtained from the ROM, which was previously validated using experimental data and CFD simulations. The dataset used for this comparison was obtained by simulating the ROM for 110 h; these data were generated using the same bounds on the input parameters P for the training dataset of 40,000 points (50 cycles) considered in the identification test. A set of 8,000 new fresh data points were recorded from the dynamic ROM to perform this comparison. Note that this dataset is different from data set used during the identification of the RNN model. Figure. 16 and Figure. 17 present typical load-following and co-

firing scenarios, respectively, which were used to evaluate the performance of the RNN. As shown in Figure. 16, the profile of each output determined by the dynamic ROM agree with those predicted by each of the RNN sub-networks. The most significant deviations are observed for the slag thickness. In this case, the dynamic response of the slag thickness shown in Figure. 16 illustrates that when fuel load starts to decrease at around 5 min, slag viscosity starts to increase due to the reduction of refractory temperature at the outlet, which leads to an increase of the slag thickness at the outlet of the gasifier. In Figure. 17 (co-firing scenario), the slag thickness starts to increase at around 15 mins from 0.0012 m to 0.0018 m since coal is added into the fuel at time 10 mins and coal has a higher ash content, which leads to an increase in the slag thickness. Both responses in slag thickness follow the behavior observed from the dynamic ROM for this variable.

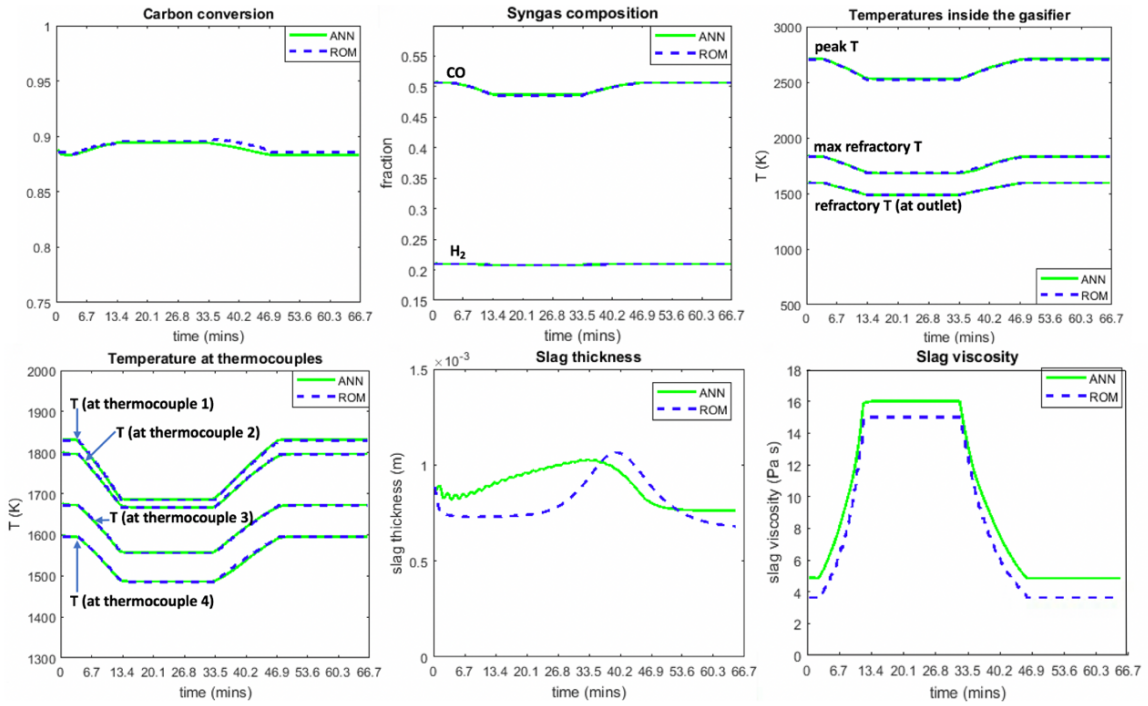

Figure 16. Identification results for load-following

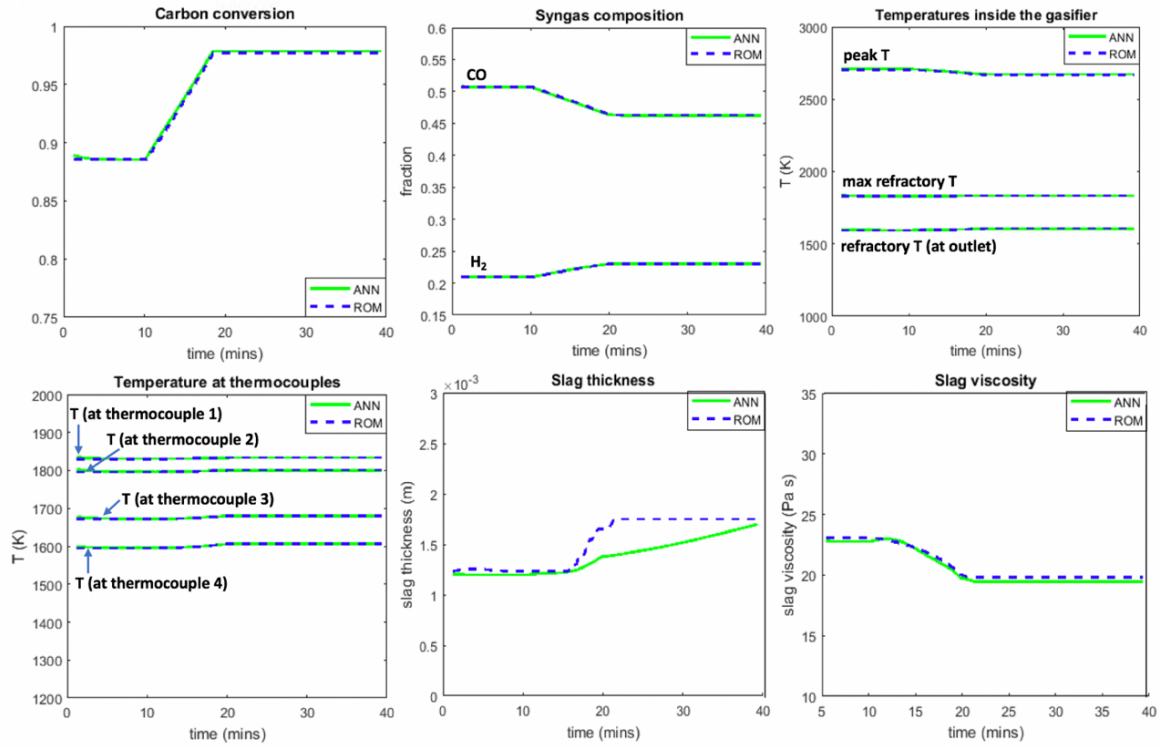

Figure 17. Identification results for co-firing

To further compare the performance of the proposed RNN model, an additional set of data involving 5 cycles like those described in Figure.15 were considered. This comparison is illustrated in Figure.18, which shows that the RNN is able to adequately capture the behavior of the gasifier unit during load-following followed by co-firing. With regards to the computational costs, the dynamic ROM and the RNN required on average 11,796 s (196.6 mins) and 0.28 s of CPU time for the load-following scenario and 4,475 s (74.58 mins) and 0.18 s of CPU time for co-firing scenario, respectively (Intel® Core™ i7-4770 CPU @ 3.40Hz, 3392 Mhz, 4 Core(s), 8 Logical Processor(s)). This difference in computational times illustrates that the RNN is able to predict the transient behavior of the gasifier approximately five orders of magnitude faster than the dynamic ROM. This demonstrates that the RNN is able to capture the overall behavior of the gasifier unit using shorter CPU times than those required by the dynamic ROM. Therefore, the RNN developed in this work can be used to perform optimization studies.

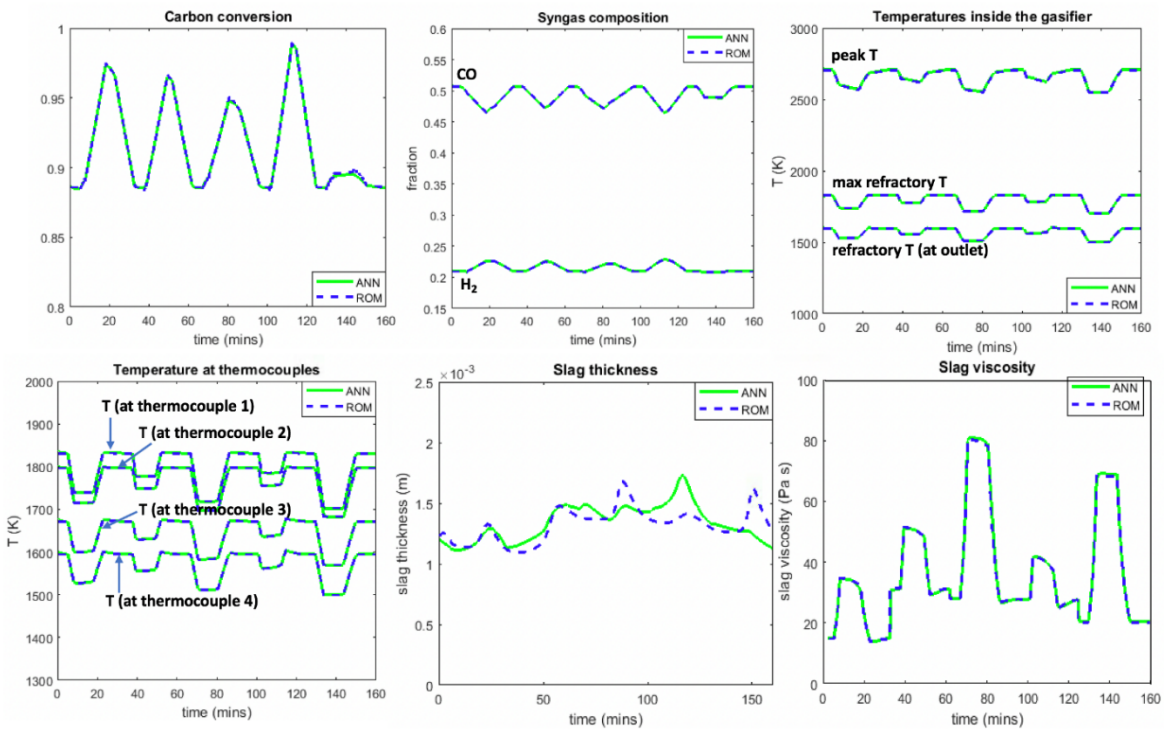

Figure 18. Identification results for combination of load-following and co-firing

4.3 Optimization: Load-following scenario

To meet the targets for seasonal and sudden changes in electricity demands, IGCC plants are required to have high flexibility to change the feed flowrate when this technology is combined with other alternative energy sources.[24] One of the metrics used to evaluate the performance of a gasification unit in an IGCC plant is the composition of the syngas at the outlet, e.g. CO. As a result, it is crucial to manufacture IGCCs that meet specific product composition requirements in order to maximize gasifier performance.[73,21] Note that the peak temperature of the gasifier reactor should be maintained below a threshold to avoid damaging the refractory wall due to the high temperature. Similarly, the slag thickness should also be maintained within an acceptable limit to avoid slag blockage at the bottom of the gasification unit.

Based on the above, the aim of this case study is to seek for the time-dependent profile in the fuel flowrate using two different objective functions (OF_j). The first objective (OF_1) aims to maximize

the mean value of composition of CO at the reactor outlet whereas the second objective (OF_2) aims to minimize sum squared errors between the composition of CO and a pre-specified target set-up point of CO at each time interval. The optimization problem under consideration can be formulated as follows:

$$\max_{\mathrm{P'}_1(t_i),\, \mathrm{P'}_5(t_i)} \; OF_j \tag{11}$$

Subject to:

$RNN\ model$

$t_i = i\Delta t;\ \forall i = 0, 1, 2, \cdots, n$

$\mathrm{P'}_1(t_0) = \ \mathrm{P}_1^{t0}$

$T_4\ (\mathbf{P}'(t_i)) \leq T_{4,max}$

$T_{12}\ (\mathbf{P}'(t_i)) \leq T_{12,max}$

$\mathbf{P}_{min} \leq\ \mathbf{P}'(t_i) \leq \mathbf{P}_{max}$

where OF_j are defined as follows:

$$OF_1 = \frac{1}{n}\sum_{i=1}^{n} T_2\big(\mathbf{P}'(t_i)\big) \tag{12}$$

$$OF_2 = \ \sum_{i=1}^{n}(T_2\big(\mathbf{P}'(t_i)\big) - \mathrm{T}_2^*) \tag{13}$$

where t_i represents the time points at which the outputs are predicted from the RNN; n is the number of time points, Δt is the length of the sampling interval; $\mathbf{P}_{min}$ and $\mathbf{P}_{max}$ represent the lower and the upper bounds for the input parameters $\mathbf{P}'$, which are listed in Table 13. As shown in Table 13, P_1^{t0} is the initial operating condition of the fuel flowrate whereas $T_{4,max}$ and $T_{12,max}$ denote the maximum allowable temperature that the refractory wall can bear and the maximum allowable thickness that avoids the blockage at the bottom of gasifier, respectively. T_2^* in (13) represents the pre-specified target set-up point for CO. The above optimization formulation was solved under three different temperature constraints, i.e., $T_{4,max}$ was set to 2,800K, 2,700K, and 2,600K. The

latter was performed to obtain insight on the sensitivity of the peak temperature constraint on the optimal solution. The maximum slag thickness ($T_{12,max}$) was set to 1.28 mm. As shown in problem (11), the RNN gasification model is used to predict the CO composition (T_2), peak temperature (T_4) and slag thickness at the outlet of gasifier (T_{12}) at each time instant by adjusting the fuel flowrate (P'_1) and limestone (CaO) flowrate (P'_5), which are the optimization variables considered for this case study. Note that P'_5 is a fluxant used to control the slag thickness inside the gasifier. The above optimization problem was implemented in Matlab 2017 and solved using the interior point algorithm available through the built-in function *fmincon*. Control vector parameterization was used to solve the nonlinear dynamic optimization problem shown in (11).

Table 15 presents the results obtained when *OF₁* is maximized using three different peak temperature limits. As shown in Table 15, the composition of CO increased slightly from 0.5319 to 0.5357 when $T_{4,max}$ was changed from 2,600 K to 2,800 K, respectively. As illustrated in Figure 19, when the maximum allowed temperature is relaxed from 2,600K to 2,800K, the time-dependent profiles for the fuel flowrate increase and reach a high fuel load condition. Note that the changes in the flue flowrate are non-trivial and follow different profiles thus illustrating the benefits of performing optimization for this process. These results also show that there exists a nonlinear correlation between the fuel load and the maximum allowed peak temperature within the gasifier. Moreover, the flowrate of CaO also increased in a nonlinear fashion from 2.7059 kg/h to 3.1946 kg/h when $T_{4,max}$ was increased from 2,600K to 2,800K, as shown in Figure.19. The results obtained for the fuel and CaO flowrates are reasonable since an increase in the fuel flowrate would cause a higher thickness of slag at the outlet of gasifier; thus, a higher CaO flowrate (fluxant) is needed for inlet of gasifier to avoid the blockage inside the gasifier. The maximum slag thickness remained below 1.28 mm (i.e., within the limitation of slag thickness) for the three peak temperature constraints considered in this study.

Table 15. CO composition optimization (OF_1) results for load-following scenario

	$T_{4,max} = 2{,}800K$	$T_{4,max} = 2{,}700K$	$T_{4,max} = 2{,}600K$
Mean value of CO composition	0.5357	0.5347	0.5319
Max peak temperature (K)	2,744	2,695	2,596
Max slag thickness (mm)	1.28	1.275	1.274

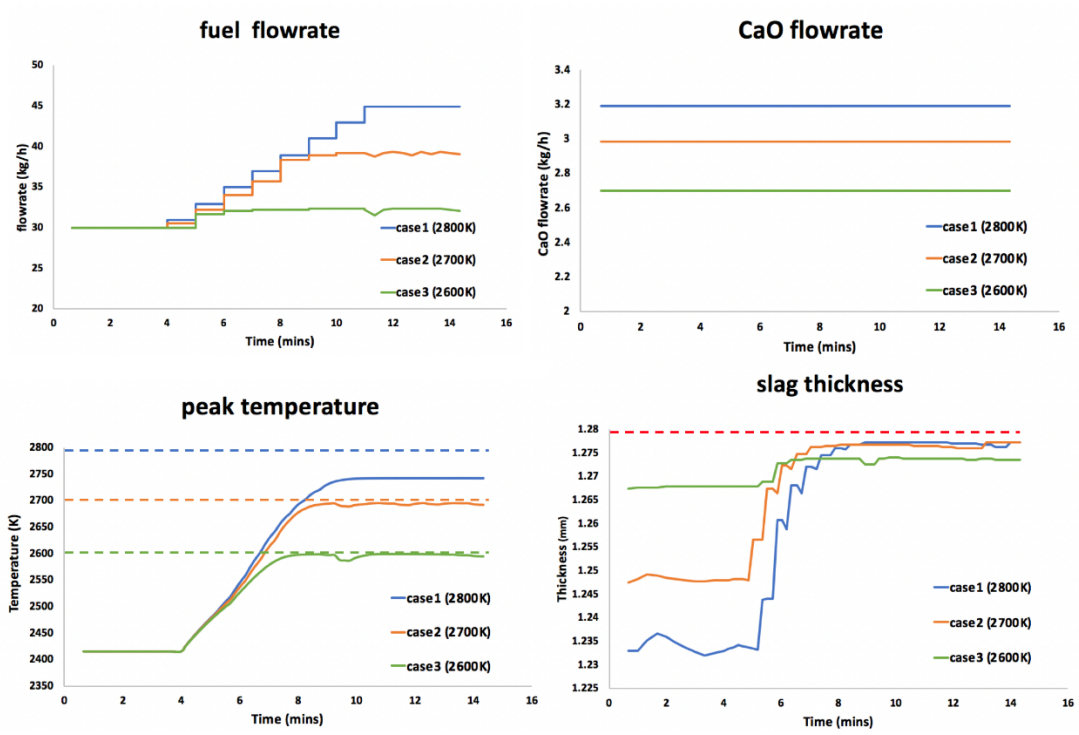

Figure 19. Optimization results for load-following scenario (OF_1)

Figure. 20 shows the results of solving problem (11) using OF_2 shown in equation (13), i.e., minimization of the sum of the squared errors. As shown in this figure, problem (11) was solved using three pre-specified set-points for the CO composition, i.e., T_2^* in equation (13) was set to 0.536, 0.534, and 0.532, respectively. To simplify the analysis, the maximum allowable temperature $\boldsymbol{T_{4,max}}$ was fixed at 2,700 K for this optimization case study whereas the maximum slag thickness was set to 1.28 mm. As shown in Figure. 20, the fuel flowrate profiles increase and reach a higher value when the pre-specified set-up point (i.e., T_2^* in (13)) was increased from 0.532 to 0.536; accordingly, the maximum peak temperature inside the gasifier increased from 2,584 K to 2,695 K, respectively. In OF_2 optimization, the CO composition slightly increases from case 1 to case 3; however, the value of fuel flowrate and peak temperature increase in a much larger scale. These result shows that both fuel flowrate and peak temperature are sensitive to the CO composition at the outlet of the gasifier and a relatively small difference in CO composition may lead to large changes on fuel flowrate and peak temperature. These results also show that there is a nonlinear relationship between fuel flowrate and CO composition, i.e. both the fuel flowrate and peak temperature exhibit non-trivial profiles that can only be obtained from optimization. The maximum slag thickness at the outlet of the gasifier increased slightly from 1.2749 mm to 1.2782 mm when the target set-up point of CO was changed from 0.532 to 0.536, respectively. Therefore, a higher CaO flowrate was needed to maintain the slag thickness within its corresponding limit. With regards to the computational costs, the average CPU time needed to solve the optimization problems for the load-following scenarios discussed above was 68 s (Intel® Core™ i7-4770 CPU @ 3.40Hz, 3392 Mhz, 4 Core(s), 8 Logical Processor(s)), which is a sufficiently low compared to the CPU time needed to simulate a single operating condition using the dynamic ROM.

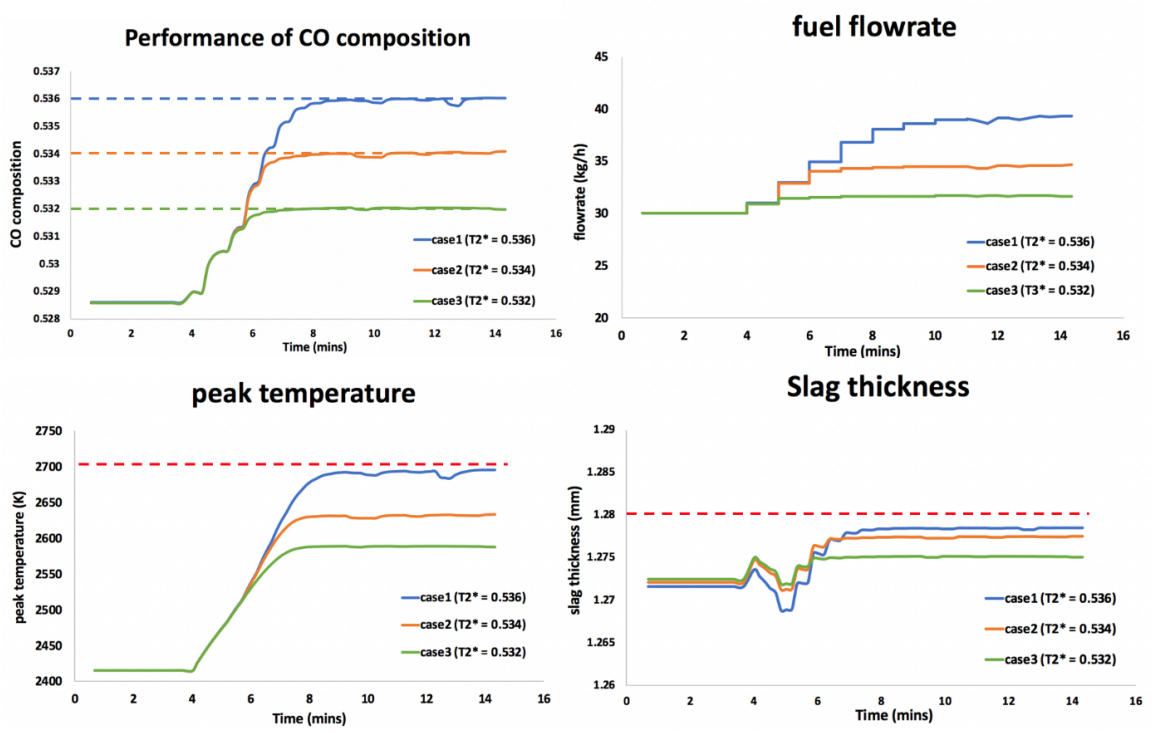

Figure 20. Optimization results for load-following scenario (OF_2)

4.4 Optimization: Co-firing scenario

IGCC power plants need to have flexibility to operate using different type of fuels.[24] Co-firing can increase the availability of the fuel and be used to reduce the costs of the plant and their footprint to the environment. In this co-firing scenario, the performance of the gasifier is assessed using the mean value of carbon conversion (T_1). Consequently, we aim to find the optimal fuel flowrate (P'_1), ratio of coal to pet-coke (θ), which represents the ratio of the blending fuel at the end of co-firing process, and the limestone flowrate (P'_5) that maximizes the mean value of carbon conversion. This optimization problem can be formulated is as follows:

$$\max_{P'_1(t_i),\theta,P'_5(t_i)} \frac{1}{n} \sum_{i=1}^{n} T_1(\mathbf{P}'(t_i)) \quad (14)$$

Subject to:

$RNN\ model$

$t_i = i\Delta t;\ \forall i = 0, 1, 2, \cdots, n$

$T_4\ (\mathbf{P}'(t_i)) \leq T_{4,max}$

$T_{12}\ (\mathbf{P}'(t_i)) \leq T_{12,max}$

$\mathbf{P}_{min} \leq\ \mathbf{P}'(t_i) \leq \mathbf{P}_{max}$

$\theta_{min} \leq\ \theta \leq \theta_{max}$

where $T_{4,max}$, $T_{12,max}$ were set to 2,700 K and 1.28 mm, respectively. During the co-firing scenario, the fuel type changes from pure pet-coke to a mixture of pet-coke and coal; therefore, upper and lower bounds for θ were set to 0 (pure pet-coke) and θ_{max}, which is the maximum ratio of coal to pet-coke that can be accomplished with the dynamic ROM. The rest of the parameters in the co-firing optimization problem (14) remained the same as in the load-following scenario described above. Also, the optimization problem (14) was solved using the same optimization procedure used to solve problem (11).

With the aim to obtain an insight on the effect of the ratio of the blending fuel on the mean value of carbon conversion, problem (14) was solved using different θ_{max} values, i.e., 0.3, 0.4, 0.5 and 0.6. Figure.21 illustrates the changes in the fuel composition and CaO flowrate. As shown in Table 16, when θ_{max} increased from 0.3 to 0.6, the average carbon conversion during co-firing increased from 94.89% to 96.81%. Thus, increasing the ratio of coal to pet-coke can lead to an increase in mean carbon conversion during co-firing. This is expected since coal has less fixed carbon and more volatiles than petroleum coke. Meanwhile, a higher limestone flowrate is needed when the coal to pet-coke ratio (θ) is increased. This is mostly because coal has higher ash composition than petroleum coke; thus, a larger CaO flowrate is needed to avoid the growth of

the slag thickness inside the gasifier's walls. The RNN-based optimization problem required on average 115 s of CPU time for the co-firing optimization scenarios considered in this study. This makes the RNN model highly attractive to perform complex studies involving the optimal operation of large-scale gasification systems.

Table 16. Carbon conversion optimization results for co-firing scenario

	Different maximum coal to pet-coke ratio (θ_{max})			
θ_{max}	0.3	0.4	0.5	0.6
Mean value of carbon conversion	0.9489	0.9559	0.9588	0.9681
Fuel flowrate (kg/h)	30.0117	30.2671	30.2036	30.2899
CaO flowrate (kg/h)	4.2537	4.3434	4.4953	4.7422
Coal to pet-coke ratio (θ)	0.2999	0.3972	0.4950	0.5959

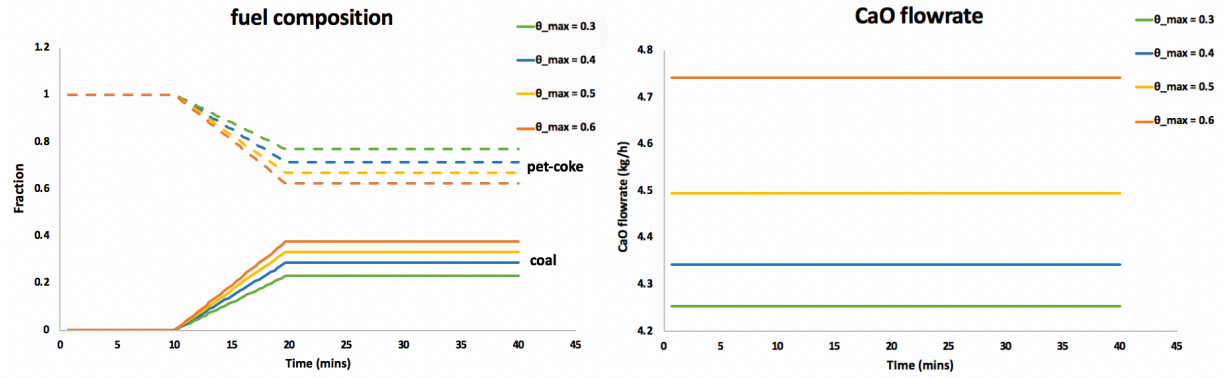

Figure 21. Optimization results for co-firing scenario

4.5 Summary

This chapter presented a systematic approach to build a recurrent neural network (RNN) that is able to predict the dynamic behavior of a pilot-scale entrained flow gasifier. The RNN was trained

by a series of input/output data generated using a new identification method that combines two of the most common transient scenarios that occur in operation. The performance of the RNN was validated using the dynamic ROM model and it was shown to be highly predictive of the transient operation of the gasifier at significantly lower computational costs. The RNN was then used to seek for the optimal time-dependent profiles in key inputs under two scenarios often found in the operation of IGCC plants, i.e., load-following and co-firing. Results from the optimization studies showed that, for the load-following scenario, increasing the maximum allowed peak temperature inside the reactor can lead to higher CO compositions at the outlet of the gasifier. Also, results from the co-firing scenario showed that an increase on the coal to pet-coke ratio can promote a higher carbon conversion inside the gasifier.

Chapter 5
Conclusions and recommendations

5.1 Conclusions

The objective of this thesis was to illustrate the potential application of artificial neural networks to describe the complex and highly nonlinear behaviour of entrained-flow gasification units. As it was presented in this thesis, the ANN and RNN designed in this study were able to obtain reasonable accurate predictions for the gasification unit and were in reasonable agreement with to the results generated by a gasifier's ROM model at a much lower computational cost. The main conclusions obtained from this work are described next.

In order to predict the important outputs of a gasification unit in IGCC plant, an artificial neural network model was presented. This ANN model consisted of eight sub-networks; the number of neurons in the hidden layer for each neural network were determined by minimizing the error between actual output and the target output. In addition, tests were performed by comparing eight different training algorithms; the Levenberg-Marquardt training algorithm was selected due to its high efficiency and reliability. The resulting ANN was able to accurately predict the gasifier outputs at significantly lower computational costs comparing to ROM. The difference between ANN and ROM in terms of computational costs illustrates that the ANN is approximately 1.6×10^5 times faster than the ROM model. The validated ANN was used to perform two different optimization studies on the pilot-scale gasification unit. From the optimization study involving the maximization of carbon conversion, the results showed that relaxing the peak temperature constraint improve carbon conversion. In the multi-objective optimization study, the utopia point approach illustrated that it is very unlikely to improve H_2 production significantly without reducing the carbon conversion within the gasifier. The results from these two optimization studies also demonstrated that the ANN model can be embedded within optimization formulations and provide acceptable

and near-optimal solutions in shorter computational times, i.e., at least four orders of magnitude faster when compared to a ROM-based optimization formulation.

A recurrent neural network model was presented to predict the dynamic behavior of the pilot-scale entrained flow gasifier. The proposed recurrent neural network model contained twelve sub-networks for each key output. The number of neurons in the hidden layer for each neural network was determined via optimization using the Levenberg-Marquardt algorithm. The performance of the RNN was compared to that obtained by the dynamic ROM model and it was shown to be highly predictive of the transient operation of the gasifier at significantly lower computational costs, i.e., approximately 5 orders of magnitude faster than the ROM model. From the optimization studies, the results for the load-following scenario showed that increasing the maximum allowed peak temperature inside the reactor would increase the CO composition at the outlet of the gasifier. Also, from the co-firing scenario, the results showed that an increase on the coal to pet-coke ratio can promote a higher carbon conversion at the outlet of the gasifier. These optimization studies also showed that the efficiency of the gasification unit can be improved if optimal (non-trivial) time-dependent profiles that satisfy key operational constraints during co-firing and load-following can be identified using optimization techniques combined with a highly predictive and computationally efficient RNN gasification model.

5.2 Recommendations

The research presented in this thesis can be extended in different ways to further advance the development and implementation of state-of-the-art optimization, on-line monitoring and control strategies for gasification units. The recommendations that can be pursued as part of the future work in this research are as follows:

- In the present work, the simulation and optimization of the gasification unit was performed using neural networks. In the future work, the implementation of the low-order gasification models connected with an IGCC plant can be explored. Integration of the neural network models with the rest of the plant would be key to assess the performance the operability and controllability of the complete IGCC plant.

- The previously proposed ROM model describing the complex performance of the gasification unit in IGCC was implemented assuming that the design was fixed. Recent studies have indicated the need to develop novel design and controls strategies that can improve the operability and performance of emerging systems in the energy sector.[11] Hence, as part of the future work, the interactions between the design and operability of the gasification unit could be considered since they can further improve the efficiency of the gasification unit. Also, integration of design and control introduces the opportunity to establish a link between conflicting objectives of steady-state economics and dynamic performance at the early stages of the process design for the gasification unit, which enables the identification of reliable and optimal designs and provide additional opportunities in pursuing the ultimate goals of sustainable environmentally-friendly process.

- The RNN model presented in this work was developed under the assumption that the gasifier operates under two of their most common scenarios, i.e., load following and co-firing. Nevertheless, there exists other scenarios that may be relevant to the operation of this unit, e.g. feed composition variability or oscillatory changes in the fuel flowrate, which is a common operation found during plant start-up or shutdown.[78] In the future work, a low-order neural

network model that can account for a wide variety of transient operating conditions for the gasifier should be considered. It is expected that such model would be more comprehensive and realistic though it may also require a significant amount of effort for their development, e.g. have access to plant and/or simulated data that can be used to build such a network.

- In this presented research, optimization studies involving carbon conversion as well as hydrogen and carbon monoxide production were performed for the gasification unit. To date, integrated gasification combined cycle (IGCC) is still a promising technology which can generate clean, affordable and secure power; however, coal-fed IGCC power plant has lower net plant efficiency comparing to natural gas combined cycle (NGCC) power plant. Therefore, in order to make IGCC technology more competitive, the development of an optimal design and operations management strategies that can take into account the rest of the IGCC units is proposed with the aim to increase the thermal efficiency and technological development of IGCC plants.

- To date, data collection is still a problem for training acceptable neural networks for gasification units. In the current study, data obtained from a pilot-scale gasifier was used to build the corresponding neural networks. Although these models are quite attractive for their low computational costs, they required a significant amount of effort for their development. The latter worsens as the complexity and size of the model increases. There are limited studies in the literature that report information on the operation of industrial-scale gasifiers. A follow-up study that is suggested as part of the future work involves the development of inexpensive low-order models, e.g. neural networks, that can predict the behaviour of commercial-scale gasifiers. The development of such

models would be key to determine suitable operating conditions that can improve the efficiency of such large-scale units.

- The results from dynamic optimization illustrate that there exists a nonlinear relationship between some process variables, e.g. large changes in the fuel flowrate are required to adjust the CO composition target by very small amounts. This shows that optimization is key since it can provide insight on the dynamic operability of this process. In the future, a model-based control scheme can be designed to maintain the operation of this process on target. For instance, the proposed controller can be formulated as a model predictive controller that can employ a neural network as the internal process model for the gasifier.
- The neural networks considered in this work does not take into account the effects of output parameters as inputs to other neural networks. Although the predictability properties of the neural networks proposed in this work was deemed acceptable. Further improvement may be achieved if the outputs of some neural networks can be used as inputs to other networks. Therefore, in the future work, the output parameters which are predicted from sub-neural network models can be considered as input parameters for prediction of other output parameters by coupling the sub-neural network models.

Reference

(1) Archer, D. Fate of Fossil Fuel CO2 in Geologic Time. **2005**, *110* (March), 1–6. https://doi.org/10.1029/2004JC002625.

(2) Banks, B.; Bigland-Pritchard, M. *What Risk? What Reward?*; 2015.

(3) University of Stavanger. *IGCC State of the Art Report*; 2010.

(4) Yuan, Y.; You, H.; Ricardez-Sandoval, L. Recent Advances on First-Principles Modeling for the Design of Materials in CO2 Capture Technologies. *Chinese J. Chem. Eng.* **2019**, *27* (7), 1554–1565. https://doi.org/10.1016/j.cjche.2018.10.017.

(5) Wang, Y.; Nian, V.; Li, H.; Yuan, J. Life Cycle Analysis of Integrated Gasification Combined Cycle Power Generation in the Context of Southeast Asia. *Energies* **2018**, *11* (6). https://doi.org/10.3390/en11061587.

(6) Monaghan, R. F. D.; Ghoniem, A. F. A Dynamic Reduced Order Model for Simulating Entrained Flow Gasifiers: Part I: Model Development and Description. *Fuel* **2012**, *91* (1), 61–80. https://doi.org/10.1016/j.fuel.2011.07.015.

(7) Jones, D.; Bhattacharyya, D.; Turton, R.; Zitney, S. E. Rigorous Kinetic Modeling and Optimization Study of a Modified Claus Unit for an Integrated Gasification Combined Cycle (IGCC) Power Plant with CO2 Capture. *Ind. Eng. Chem. Res.* **2012**, *51* (5), 2362–2375. https://doi.org/10.1021/ie201713n.

(8) Chui, E. H.; Majeski, A. J.; Lu, D. Y.; Hughes, R.; Gao, H.; McCalden, D. J.; Anthony, E. J. Simulation of Entrained Flow Coal Gasification. *Energy Procedia* **2009**, *1* (1), 503–509. https://doi.org/10.1016/j.egypro.2009.01.067.

(9) Fletcher, D. F.; Joseph, S. D. A CFD Based Combustion Model of an Entrained Flow Biomass Gasifier. **2006**, *24* (2000), 165–182.

(10) Fletcher, D. F.; Haynes, B. S.; Chen, J.; Joseph, S. D. Computational Fluid Dynamics Modelling of an Entrained Flow Biomass Gasifier. *Appl. Math. Model.* **1998**, *22* (10), 747–

757. https://doi.org/10.1016/S0307-904X(98)10025-2.

(11) Rafiei, M.; Ricardez-Sandoval, L. A. New Frontiers, Challenges, and Opportunities in Integration of Design and Control for Enterprise-Wide Sustainability. *Comput. Chem. Eng.* **2020**, *132*. https://doi.org/10.1016/j.compchemeng.2019.106610.

(12) Sahraei, M. H.; Duchesne, M. A.; Yandon, R.; Majeski, A.; Hughes, R. W.; Ricardez-sandoval, L. A. Reduced Order Modeling of a Short-Residence Time Gasifier. **2015**, *161*, 222–232. https://doi.org/10.1016/j.fuel.2015.07.096.

(13) Sahraei, M. H.; Duchesne, M. A.; Boisvert, P. G.; Hughes, R. W.; Ricardez-Sandoval, L. A. Reduced Order Modeling of a Commercial-Scale Gasifier Using a Multielement Injector Feed System. *Ind. Eng. Chem. Res.* **2017**, *56* (25), 7285–7300. https://doi.org/10.1021/acs.iecr.7b00693.

(14) Plimmer, G.; Bryson, J.; Teo, S. T. T. Opening the Black Box: The Mediating Roles of Organisational Systems and Ambidexterity in the HRM-Performance Link in Public Sector Organisations. *Pers. Rev.* **2017**, *46* (7), 1434–1451. https://doi.org/10.1108/PR-10-2016-0275.

(15) Chaffart, D.; Ricardez-Sandoval, L. A. Optimization and Control of a Thin Film Growth Process: A Hybrid First Principles/Artificial Neural Network Based Multiscale Modelling Approach. *Comput. Chem. Eng.* **2018**, *119*, 465–479. https://doi.org/10.1016/j.compchemeng.2018.08.029.

(16) Kimaev, G.; Ricardez-Sandoval, L. A. Nonlinear Model Predictive Control of a Multiscale Thin Film Deposition Process Using Artificial Neural Networks. *Chem. Eng. Sci.* **2019**, *207*, 1230–1245. https://doi.org/10.1016/j.ces.2019.07.044.

(17) Venkatasubramanian, V. The Promise of Artificial Intelligence in Chemical Engineering: Is It Here, Finally? *AIChE J.* **2019**, *65* (2), 466–478. https://doi.org/10.1002/aic.16489.

(18) Petrescu, L.; Cormos, C. C. Environmental Assessment of IGCC Power Plants with Pre-

Combustion CO2 Capture by Chemical & Calcium Looping Methods. *J. Clean. Prod.* **2017**, *158*, 233–244. https://doi.org/10.1016/j.jclepro.2017.05.011.

(19) Phillips, J. *Integrated Gasification Capture*; 2005.

(20) Christou, C.; Hadjipaschalis, I.; Poullikkas, A. Assessment of Integrated Gasification Combined Cycle Technology Competitiveness. *Renew. Sustain. Energy Rev.* **2008**, *12* (9), 2452–2464. https://doi.org/10.1016/j.rser.2007.06.010.

(21) Kunze, C.; Spliethoff, H. Modelling of an IGCC Plant with Carbon Capture for 2020. *Fuel Process. Technol.* **2010**, *91* (8), 934–941. https://doi.org/10.1016/j.fuproc.2010.02.017.

(22) Huang, Y.; Rezvani, S.; McIlveen-Wright, D.; Minchener, A.; Hewitt, N. Techno-Economic Study of CO2 Capture and Storage in Coal Fired Oxygen Fed Entrained Flow IGCC Power Plants. *Fuel Process. Technol.* **2008**, *89* (9), 916–925. https://doi.org/10.1016/j.fuproc.2008.03.002.

(23) Ordorica-Garcia, G.; Douglas, P.; Croiset, E.; Zheng, L. Technoeconomic Evaluation of IGCC Power Plants for CO2 Avoidance. *Energy Convers. Manag.* **2006**, *47* (15–16), 2250–2259. https://doi.org/10.1016/j.enconman.2005.11.020.

(24) Sahraei, M. H.; Duchesne, M. A.; Hughes, R. W.; Ricardez-sandoval, L. A. Dynamic Reduced Order Modeling of an Entrained-Flow Slagging Gasifier Using a New Recirculation Ratio Correlation. *Fuel* **2017**, *196*, 520–531. https://doi.org/10.1016/j.fuel.2017.01.079.

(25) Sahraei, M. H.; McCalden, D.; Hughes, R.; Ricardez-Sandoval, L. A. A Survey on Current Advanced IGCC Power Plant Technologies, Sensors and Control Systems. *Fuel* **2014**, *137*, 245–259. https://doi.org/10.1016/j.fuel.2014.07.086.

(26) CanmetENERGY research service. <http://www.nrcan.gc.ca/sites/www.nrcan.gc.ca/files/canmetenergy/files/pubs/Gasification_eng.pdf> [Cited 12.01.15].

(27) Emun, F.; Gadalla, M.; Majozi, T.; Boer, D. Integrated Gasification Combined Cycle

(IGCC) Process Simulation and Optimization. *Comput. Chem. Eng.* **2010**, *34* (3), 331–338. https://doi.org/10.1016/j.compchemeng.2009.04.007.

(28) Gnanapragasam, N.; Reddy, B.; Rosen, M. Reducing CO2 Emissions for an IGCC Power Generation System : Effect of Variations in Gasifier and System Operating Conditions. *Energy Convers. Manag.* **2009**, *50* (8), 1915–1923. https://doi.org/10.1016/j.enconman.2009.04.017.

(29) Klara, J. M.; Plunkett, J. E. The Potential of Advanced Technologies to Reduce Carbon Capture Costs in Future IGCC Power Plants. *Int. J. Greenh. Gas Control* **2010**, *4* (2), 112–118. https://doi.org/10.1016/j.ijggc.2009.10.006.

(30) Wang, Y.; Qiu, P.; Wu, S.; Li, Z. Performance of an Integrated Gasification Combined Cycle System with Different System Integration Options. *Energy and Fuels* **2010**, *24* (3), 1925–1930. https://doi.org/10.1021/ef901235p.

(31) Xue, Q.; Fox, R. O. Multi-Fluid CFD Modeling of Biomass Gasification in Polydisperse Fluidized-Bed Gasifiers. *Powder Technol.* **2014**, *254*, 187–198. https://doi.org/10.1016/j.powtec.2014.01.025.

(32) Slezak, A.; Kuhlman, J. M.; Shadle, L. J.; Spenik, J.; Shi, S. CFD Simulation of Entrained-Flow Coal Gasification: Coal Particle Density/Sizefraction Effects. *Powder Technol.* **2010**, *203* (1), 98–108. https://doi.org/10.1016/j.powtec.2010.03.029.

(33) Yong, S. Z.; Ghoniem, A. Modeling the Slag Layer in Solid Fuel Gasification and Combustion :Two-Way Coupling with CFD. *Fuel* **2012**, *97*, 457–466. https://doi.org/10.1016/j.fuel.2012.02.063.

(34) Fernando, N.; Narayana, M. A Comprehensive Two Dimensional Computational Fluid Dynamics Model for an Updraft Biomass Gasifier. *Renew. Energy* **2016**, *99*, 698–710. https://doi.org/10.1016/j.renene.2016.07.057.

(35) Murgia, S.; Vascellari, M.; Cau, G. Comprehensive CFD Model of an Air-Blown Coal-

Fired Updraft Gasifier. *Fuel* **2012**, *101*, 129–138. https://doi.org/10.1016/j.fuel.2011.08.065.

(36) Lee, H. H.; Lee, J. C.; Joo, Y. J.; Oh, M.; Lee, C. H. Dynamic Modeling of Shell Entrained Flow Gasifier in an Integrated Gasification Combined Cycle Process. *Appl. Energy* **2014**, *131*, 425–440. https://doi.org/10.1016/j.apenergy.2014.06.044.

(37) Lee, H.; Lee, J. H. Multiloop Control Strategies for a Dry Feeding Gasifier in the Integrated Gasification Combined Cycle. *Ind. Eng. Chem. Res.* **2015**, *54* (44), 11113–11125. https://doi.org/10.1021/acs.iecr.5b01797.

(38) Gazzani, M.; Manzolini, G.; MacChi, E.; Ghoniem, A. F. Reduced Order Modeling of the Shell-Prenflo Entrained Flow Gasifier. *Fuel* **2013**, *104*, 822–837. https://doi.org/10.1016/j.fuel.2012.06.117.

(39) Yang, Z.; Wang, Z.; Wu, Y.; Li, Z.; Ni, W. Use of a Reactor Network Model in the Design and Operation of a New Type of Membrane Wall Entrained Flow Gasifier. *Energy and Fuels* **2013**, *27* (10), 6322–6332. https://doi.org/10.1021/ef401451f.

(40) Yang, Z.; Wang, Z.; Wu, Y.; Wang, J.; Lu, J.; Li, Z.; Ni, W. Dynamic Model for an Oxygen-Staged Slagging Entrained Flow Gasifier. *Energy and Fuels* **2011**, *25* (8), 3646–3656. https://doi.org/10.1021/ef200742s.

(41) Li, C.; Dai, Z.; Sun, Z.; Wang, F. Modeling of an Opposed Multiburner Gasifier with a Reduced-Order Model. *Ind. Eng. Chem. Res.* **2013**, *52* (16), 5825–5834. https://doi.org/10.1021/ie3030505.

(42) Wang, H.; Chaffart, D.; Ricardez-Sandoval, L. A. Modelling and Optimization of a Pilot-Scale Entrained-Flow Gasifier Using Artificial Neural Networks. *Energy* **2019**, *188*, 116076. https://doi.org/10.1016/j.energy.2019.116076.

(43) Pirdashti, M.; Curteanu, S.; Kamangar, M. H.; Hassim, M. H.; Khatami, M. A. Artificial Neural Networks: Applications in Chemical Engineering. *Rev. Chem. Eng.* **2013**, *29* (4),

205–239. https://doi.org/10.1515/revce-2013-0013.

(44) Dayhoff, J. E.; Deleo, J. M. *Opening the Black Box*; 2001.

(45) Davidian, D. *Feed-Forward Neural Network*; 1995.

(46) Ongen, A.; Kurtulus Ozcan, H.; Arayici, S. An Evaluation of Tannery Industry Wastewater Treatment Sludge Gasification by Artificial Neural Network Modeling. *J. Hazard. Mater.* **2013**, *263*, 361–366. https://doi.org/10.1016/j.jhazmat.2013.03.043.

(47) Mikulandric, R. Artificial Neural Network Modelling Approach for a Biomass Gasification Process in Fixed Bed Gasifiers. **2014**, *87*, 1210–1223. https://doi.org/10.1016/j.enconman.2014.03.036.

(48) Puig-Arnavat, M.; Hernández, J. A.; Bruno, J. C.; Coronas, A. Artificial Neural Network Models for Biomass Gasification in Fluidized Bed Gasifiers. *Biomass and Bioenergy* **2013**, *49*, 279–289. https://doi.org/10.1016/j.biombioe.2012.12.012.

(49) Guo, B.; Li, D.; Cheng, C.; Lü, Z. A.; Shen, Y. Simulation of Biomass Gasification with a Hybrid Neural Network Model. *Bioresour. Technol.* **2001**, *76* (2), 77–83. https://doi.org/10.1016/S0960-8524(00)00106-1.

(50) George, J.; Arun, P.; Muraleedharan, C. Assessment of Producer Gas Composition in Air Gasification of Biomass Using Artificial Neural Network Model. *Int. J. Hydrogen Energy* **2018**, *43* (20), 9558–9568. https://doi.org/10.1016/j.ijhydene.2018.04.007.

(51) Connor, J. T.; Martin, R. D.; Atlas, L. E.; Ieee, M. Recurrent Neural Networks and Robust Time Series Prediction. **1994**, *5* (2), 240–254.

(52) Williams, R. J.; Peng, J. An Efficient Gradient-Based Algorithm for On-Line Training of Recurrent Network Trajectories. *Neural Comput.* **1990**, *2* (4), 490–501. https://doi.org/10.1162/neco.1990.2.4.490.

(53) Hasim, S.; Senior, A.; Francoise, B. *Long Short-Term Memory Recurrent Neural Network Architectures for Large Scale Acoustic Modeling*.

(54) Cheng, C. H.; Ye, J. X. GA-Based Neural Network for Energy Recovery System of the Electric Motorcycle. *Expert Syst. Appl.* **2011**, *38* (4), 3034–3039. https://doi.org/10.1016/j.eswa.2010.08.093.

(55) Sekhar, V.; Ravi, K. Low-Voltage Ride-through Capability Enhancement of Wind Energy Conversion System Using an Ant-Lion Recurrent Neural Network Controller. *Meas. Control* **2019**, *52* (7–8), 1048–1062. https://doi.org/10.1177/0020294019858102.

(56) De Souza, M. B.; Barreto, A. G.; Nemer, L. C.; Soares, P. O.; Quitete, C. P. B. A Study on Modeling and Operational Optimization of Biomass Gasification Processes Using Neural Networks. In *AIChE Annual Meeting, Conference Proceedings*; 2010.

(57) Pandey, D. S.; Das, S.; Pan, I.; Leahy, J. J.; Kwapinski, W. Artificial Neural Network Based Modelling Approach for Municipal Solid Waste Gasification in a Fluidized Bed Reactor. *Waste Manag.* **2016**, *58*, 202–213. https://doi.org/10.1016/j.wasman.2016.08.023.

(58) Roy, K.; Mandal, K. K.; Mandal, A. C. Modeling and Managing of Micro Grid Connected System Using Improved Artificial Bee Colony Algorithm. *Int. J. Electr. Power Energy Syst.* **2016**, *75*, 50–58. https://doi.org/10.1016/j.ijepes.2015.08.003.

(59) Mikulandrić, R.; Lončar, D.; Böhning, D.; Böhme, R.; Beckmann, M. Artificial Neural Network Modelling Approach for a Biomass Gasification Process in Fixed Bed Gasifiers. *Energy Convers. Manag.* **2014**, *87*, 1210–1223. https://doi.org/10.1016/j.enconman.2014.03.036.

(60) Wang, J.; Wan, W. Application of Desirability Function Based on Neural Network for Optimizing Biohydrogen Production Process. *Int. J. Hydrogen Energy* **2009**, *34* (3), 1253–1259. https://doi.org/10.1016/j.ijhydene.2008.11.055.

(61) Kalogirou, S. A. Optimization of Solar Systems Using Artificial Neural-Networks and Genetic Algorithms. *Appl. Energy* **2004**, *77* (4), 383–405. https://doi.org/10.1016/S0306-

2619(03)00153-3.

(62) Wang, J.; Sun, Z.; Dai, Y.; Ma, S. Parametric Optimization Design for Supercritical CO2 Power Cycle Using Genetic Algorithm and Artificial Neural Network. *Appl. Energy* **2010**, *87* (4), 1317–1324. https://doi.org/10.1016/j.apenergy.2009.07.017.

(63) Duch, W.; Jankowski, N. Transfer Functions: Hidden Possibilities for Better Neural Networks. In *9th European Symposium on Artificial Neural Networks*; 2001; pp 81–94.

(64) Ilonen, J.; Kamarainen, J. K.; Lampinen, J. Differential Evolution Training Algorithm for Feed-Forward Neural Networks. *Neural Process. Lett.* **2003**, *17* (1), 93–105. https://doi.org/10.1023/A:1022995128597.

(65) Luyben, W. L.; Robinson, P. J. A Simple Gasifier Model That Runs in Aspen Dynamics. In *AIChE Annual Meeting, Conference Proceedings*; 2008; pp 7784–7792.

(66) Chui, E. H.; Majeski, A. J.; Lu, D. Y.; Hughes, R.; Gao, H.; McCalden, D. J.; Anthony, E. J. Simulation of Entrained Flow Coal Gasification. *Energy Procedia* **2009**, *1* (1), 503–509. https://doi.org/10.1016/j.egypro.2009.01.067.

(67) Ning Wang; Meng Joo Er; Min Han. Generalized Single-Hidden Layer Feedforward Networks for Regression Problems. *IEEE Trans. Neural Networks Learn. Syst.* **2014**, *26* (6), 1161–1176. https://doi.org/10.1109/tnnls.2014.2334366.

(68) Wechsler, H. *Computation, Learning, and Architectures*; 1992; Vol. 2.

(69) Kuldip Vora, S. Y. A Survey on Backpropagation Algorithms for Feedforward Neural Networks. *Int. J. Eng. Dev. Res.* **2014**, *1* (3), 193–197.

(70) Maier, H. R.; Dandy, G. C. Understanding the Behaviour and Optimising the Performance of Back-Propagation Neural Networks : An Empirical Study; 1998; Vol. 13, pp 179–191.

(71) Ozkaya, B.; Demir, A.; Bilgili, M. S. Neural Network Prediction Model for the Methane Fraction in Biogas from Field-Scale Landfill Bioreactors. *Environ. Model. Softw.* **2007**, *22* (6), 815–822. https://doi.org/10.1016/j.envsoft.2006.03.004.

(72) Charry-Sanchez, J.; Betancourt-Torcat, A.; Ricardez-Sandoval, L. An Optimization Energy Model for the Upgrading Processes of Canadian Unconventional Oil. *Energy* **2014**, *68*, 629–643. https://doi.org/10.1016/j.energy.2014.03.016.

(73) McKendry, P. Energy Production from Biomass (Part 3): Gasification Technologies. *Bioresour. Technol.* **2002**, *83* (1), 55–63. https://doi.org/10.1016/s0960-8524(01)00120-1.

(74) Yeon, D.; Fukasawa, R.; Ricardez-sandoval, L. Bi-Objective Short-Term Scheduling in a Rolling Horizon Framework : A Priori Approaches with Alternative Operational Objectives. *Comput. Oper. Res.* **2019**. https://doi.org/10.1016/j.cor.2019.06.006.

(75) Wang, H.; Ricardez-Sandoval, L. A. Dynamic Optimization of a Pilot-Scale Entrained-Flow Gasifier Using Artificial Recurrent Neural Networks. *Fuel* (submitted for publication).

(76) Wang, P.; Massoudi, M. Slag Behavior in Gasifiers. Part I: Influence of Coal Properties and Gasification Conditions. **2013**, 784–806. https://doi.org/10.3390/en6020784.

(77) Pedersen, L. S.; Breithaupt, P.; Dam-Johansen, K.; Weber, R. Residence Time Distributions in Confined Swirling Flames. *Combust. Sci. Technol.* **1997**, *127* (1–6), 251–273. https://doi.org/10.1080/00102209708935696.

(78) Henderson, C. Increasing the Flexibility of Coal-Fired Power Plants. IEA Clean Coal Centre 2014.

(79) Ilyushechkin, A. Y.; Hla, S. S.; Roberts, D. G.; Kinaev, N. N. The Effect of Solids and Phase Compositions on Viscosity Behaviour and TCV of Slags from Australian Bituminous Coals. *J. Non. Cryst. Solids* **2011**, *357* (3), 893–902. https://doi.org/10.1016/j.jnoncrysol.2010.12.004.

(80) Williams, R. J.; Zipser, D. *Gradient-Based Learning Algorithms for Recurrent Networks and Their Computational Complexity Introduction*; 1995.

(81) Wysocki, A.; Ławry, M. Jordan Neural Network for Modelling and Predictive Control of Dynamic Systems. *2015 20th Int. Conf. Methods Model. Autom. Robot.* **2015**, *2* (1), 145–

150. https://doi.org/10.1109/MMAR.2015.7283862.